UNIVERSALITY IN ONE-DIMENSIONAL NONEQUILIBRIUM SYSTEMS WITH BOUNDARIES

Horatiu Simon

Abstract: The mean-field description of the steady state of the fully asymmetric exclusion model is derived. The boundary induced phases can be thus properly obtained.

The coagulation $(A + A \to A)$ model on a one-dimensional lattice opened at one end and with an input of particles at the other end is considered. For some choices of the reaction rates, exact solutions for the particle concentration in the steady state are given. They are compared with the concentration profiles for other rates obtained through Monte Carlo simulations. For large distances away from the source the concentrations coincide. This is the first example of universality in stationary states with boundaries.

A condition satisfied by similarity transformations which yield mappings between different reaction-diffusion system is derived. Several examples are given.

Contents

Chapter 1

Introduction

Diffusion controlled reactions in low dimensional systems have attracted much interest in the last years. They are non-equilibrium statistical systems which exhibit the property of self-organization. Theoretical descriptions have to take into account local fluctuations in the particle density. Mean field equations usually fail to reproduce the dynamics of these models which are characterized by non-trivial correlations.

There is a small number of *exactly solvable* models for which rigorous results were derived. The great interest in solvable models comes from the fact that their physical properties appear also in many other more complicated models.

The continuous time evolution of the systems is determined by a master equation [1]. It is useful to rewrite this last mentioned equation as a Euclidian Schrödinger equation [2]. This can be done because one deals with a first order (in time derivatives), linear and homogeneous system of equations which determines the probability distribution of the systems.

In this work we will consider one-dimensional two-state models (i.e. models with only one species of particles and vacancies).

The most important results concerning the time evolution of the particle concentration were obtained for the annihilation model and for the coagulation model. It is a well known fact that the two models are equivalent [3, 4, 5]. Both models describe particles which diffuse stochastically. When two particles meet at the same place they react. In the coagulation model they coalesce to a single one ($A + A \to A$) and in the annihilation model they both leave the system ($A + A \to 0$). For a possible experimental realization see [6] and the discussion at the beginning of Chapter 3.

The annihilation model defined on a one-dimensional lattice was solved exactly for a special choice of the reaction rates [7, 2]. In this case the linear operator appearing in the master equation can be diagonalized explicitly. The first class contains mainly models with an underlying theory of free fermions. We will come back to this point in Section 4.2.1.

The theoretical study of coagulation models defined in a d-dimensional space has a long history. It started with the observation that the critical dimension of the corresponding field theory is $d_c = 2$ [4]. A breakthrough towards the exact solution of the one-dimensional coagulation model on a lattice was the introduction of so-called interparticle distribution functions (IPDF's)[8]-[13]. For certain choices of the rates of the reactions (3.0.10), the IPDF formalism leads to a hierarchy of differential equations which decouple similarly as those obtained for the Glauber model [14]. We will come back to this point in Section 3.1.1. The most general conditions for the decoupling to occur and the corresponding spectrum in the one-hole sector are given in Ref. [15]. The models for which the spectrum of the Hamiltonian can be written in terms of free fermions can be mapped on systems which fulfill these conditions. For some "partially integrable" systems, exact results can be obtained because the decoupling occurs although the spectrum of the corresponding Hamiltonian is not the one of free fermions [15].

The steady state properties of diffusion (or exclusion) models with particle input and output at the boundaries have been studied with the help of algebraic techniques [16]-[20]. The corresponding probability distribution can be exactly computed in terms of matrix elements of products of operators in some auxiliary space [17]. The ansatz, as it is formulated in References [17] and [20], can be applied in the case of system in which the only process allowed in the bulk of the lattice is particle diffusion [21]. If more bulk reactions are included, only the cases with factorized steady states can be determined [20].

The present work is dedicated to the study of the *universality* properties of several one-dimensional reaction diffusion systems. In the definition of these models two types of parameters enter. On one hand there are the rates of the reaction processes which determine the dynamics of these stochastic systems. On the other hand, if one is interested in the time evolution, the solution of the master equation depends on the parameters defining the initial state of the system.

A physical observable can depend on, respectively can be independent of a specifical parameter. We determine different physical quantities with the help of analytical and numerical methods. In doing so, our goal is to divide the set of parameters with respect to the simple principle mentioned above.

The fully asymmetric exclusion (FAE) model is the simplest example of a reaction-diffusion system which presents boundary induced phase transitions. In Chapter 2 we give, for the first time in the literature, the complete derivation of the mean field description of the steady state of the (FAE) model. Afterwards we use the opportunity to compare this results with the exact solution [16]-[19].

We will show that surprisingly many properties of the system can be derived by using the mean field analysis. This includes predictions concerning the universality of the particle current and concentration. The FAE model is not the only one for which many mean field results are confirmed by the exact solution. This happens also in the case of the steady state properties of the model presented in Chapter 3.

The one-dimensional coagulation model with spatial *homogeneous* external particle input at all sites has been studied extensively [22, 23] and algebraic relaxation times have been observed. In Chapter 3 we investigate the same model with open boundary conditions and *localized* particle input at the ends of the chain. This model has been considered for the first time in the mean-field approximation in Ref. [24]. In the present work we compute the particle concentration in the stationary state. This can not be done with the help of the above mentioned matrix product techniques [25]. We show that by making the computations for the model with particle input at only one end, we solve the general problem in which particles enter the systems at both boundary points. We give the full solution on the lattice and in the continuum. Several universality properties of the particle concentration are proven. As mentioned before, exact solutions can be given only for special choices of the rates of the reactions happening in the bulk of the system. We investigate the universality properties of the systems for which no exact results are available with the help of Monte Carlo simulations. The main motivation of this Chapter stems from the observation that in the mean field approximation (to be reviewed later) the density of particles has an algebraic decay and one can look for universality properties.

It is the first time that universality properties of the stationary state of one-dimensional reaction-diffusion systems with boundaries are proven. We show that phenomena like finite-size scaling of the particle concentration and algebraic decay of the same observable occur even if the time relaxation spectrum is massive.

In the Appendices A and B we prove some results presented in Chapter 3. Appendix C contains details about the above mentioned Monte Carlo simulations.

Chapter 4 contains a algebraic and a numerical study. The motivation of this Chapter stems from the observation that the annihilation model can be used to explain some experimentally measured time series [6].

In section 4.2 we look for the universality classes of exactly solved models. We use local similarity transformations which yield mappings between different one-dimensional reaction-diffusion systems. Two reaction-diffusion models are in the same universality class when there exists such a local similarity transformation which allows the computation of the expectation value of any operator in one model as a linear combination of expectation values of operators in the other model. In this way results obtained for special systems can be generalized to the reaction-diffusion models contained in the same universality class. The coagulation or the annihilation models can be mapped onto systems in which both processes are allowed. With the help of the coagulation-decoagulation model, results for some death-decoagulation and annihilation-creation systems are given. We also find a reaction-diffusion system which is equivalent to the two species annihilation model ($A + B \rightarrow \emptyset$).

Besides that, in section 4.3 we present another set of numerical results of Monte Carlo simulations. An accurate description of the effects of the reaction rates on the concentration in one-species diffusion-annihilation model is made. The asymptotic behavior of the concentration in the two species annihilation system ($A + B \rightarrow \emptyset$) with symmetric initial conditions is studied.

Most of our results were previously published. Chapter 3 is based on a article written in collaboration with Haye Hinrichsen from The Weizmann Institute of Science, Rehovot, Israel and with Vladimir Rittenberg [26]. The results presented in Chapter 4 were also published [27].

In the rest of this introductory chapter a brief review of the “Hamiltonian” formalism is given.

1.1 Reaction-Diffusion systems and the master equation

We begin with a brief review of the ”Hamiltonian” [1] description of reaction-diffusion systems. We will use the same notations and conventions as in [13, 15] where a comprehensive description of this formalism is given.

First one has to construct the configuration space. Hard core interactions among particles moving on the one-dimensional lattice are considered. This also means that multiple occupation of sites is not allowed. If the system is populated with one species of particles, each site can be either empty or occupied by one particle. If there are two species of particles each site can be in one of three states. The number of states is denoted by N and the lattice length by L. To each site i we attach a N-dimensional vector space V_i. In the two state models ($N = 2$) the vector $(\,1,\ 0\,)$ corresponds to a vacancy while the vector $(\,0,\ 1\,)$ corresponds to a occupation of the site by an A particle. In the three state models ($N = 3$) the vectors $(\,1,\ 0,\ 0\,)$, $(\,0,\ 1,\ 0\,)$ and $(\,0,\ 0,\ 1\,)$ correspond to an empty site and to occupation of the site by a particle A or B respectively.

The configuration space has the structure of an L-fold tensor product $V = V_1 \otimes \cdots \otimes V_L$. Each of the N^L vectors of the tensor product base corresponds to a possible configuration of the lattice. A natural convention used to denote these vectors is obtained by associating to each site a variable β_i which takes integer values between 0 and $N-1$. In the two state models we use $\beta_i = 0$ to index a vacancy while $\beta_i = 1$ corresponds to the presence of an A particle. In addition, $\beta_i = 2$ is used to describe a site that is occupied by a B particle, in the three state models. In this 'spin basis' [1]

$$|\{\beta\}\rangle = |\beta_1, \ldots, \beta_L\rangle \tag{1.1.1}$$

we define the ket vector

$$|P\rangle = \sum_{\{\beta\}} P(\{\beta\};t)|\{\beta\}\rangle \tag{1.1.2}$$

which describes the state of the system. $P(\{\beta\};t)$ stands for the realization probability of the configuration $\{\beta\} = \{\beta_1, \ldots, \beta_L\}$ at time t.

Alternatively, the state of a system can also be described by the set of empty intervals probabilities [23]. They are defined as the probabilities to find one or more sequences of consecutive vacant sites. This description sometimes simplifies exact computations.

The dynamics of reaction-diffusion systems are determined by the rates of the allowed processes. We consider reactions which can take place when two hopping particles collide. So the set of parameters describing the dynamics induced by the bulk processes is given by the probabilities that a state (α, β) on two adjacent sites will change into the state (γ, δ) after one unit of time, denoted by

$$\Gamma^{\alpha,\beta}_{\gamma,\delta} \quad \text{with the convention} \quad \Gamma^{\alpha,\beta}_{\alpha,\beta} = 0. \tag{1.1.3}$$

Here α, β, γ and δ take values between 0 and $N-1$. We consider the case of a homogeneous lattice, i.e. the rates are independent of the position of the pair of sites where the reaction takes place. The sum of all reaction rates which modify the state (α, β) of two neighboring sites is denoted by

$$\Gamma_{\alpha,\beta} = \sum_{\gamma,\delta=0}^{N-1} \Gamma^{\alpha,\beta}_{\gamma,\delta}\ . \tag{1.1.4}$$

All rates are non-negative, constant and real. For one species systems a list of reactions and corresponding rates is given below:

diffusion to the right	$A + \emptyset \to \emptyset + A$	rate Γ^{10}_{01}
diffusion to the left	$\emptyset + A \to A + \emptyset$	rate Γ^{01}_{10}
coagulation at the left	$A + A \to \emptyset + A$	rate Γ^{11}_{01}
coagulation at the right	$A + A \to A + \emptyset$	rate Γ^{11}_{10}
decoagulation at the right	$A + \emptyset \to A + A$	rate Γ^{10}_{11}
decoagulation at the left	$\emptyset + A \to A + A$	rate Γ^{01}_{11}
annihilation	$A + A \to \emptyset + \emptyset$	rate Γ^{11}_{00}
creation	$\emptyset + \emptyset \to A + A$	rate Γ^{00}_{11}
death at the right	$\emptyset + A \to \emptyset + \emptyset$	rate Γ^{01}_{00}
death at the left	$A + \emptyset \to \emptyset + \emptyset$	rate Γ^{10}_{00}
birth at the right	$\emptyset + \emptyset \to \emptyset + A$	rate Γ^{00}_{01}.
birth at the left	$\emptyset + \emptyset \to A + \emptyset$	rate Γ^{00}_{10}.

We will consider also some models in which, in addition to this two-sites processes, particles may be allowed to leave or enter the system at the two endpoints ($i = 1$ and $i = L$) of the lattice. We denote the corresponding rates with

$$\begin{array}{lccc} \text{input of particles} & \emptyset \to A & \text{with } \Gamma_l^{01} & \text{respectively } \Gamma_r^{01} \\ \text{output of particles} & A \to \emptyset & \text{with } \Gamma_l^{10} & \text{respectively } \Gamma_r^{10} \end{array}$$

The lower index (l respectively r) stands for the left, ($i = 1$) respectively right ($i = L$) end-site where the process takes place.

Only models with random sequential updates are studied, i.e. continuous time evolution is assumed. The master equation [1] describing the time evolution of the probability distribution $P(\{\beta\}; t)$ can be written in the form of a Euclidian Schrödinger equation [2]

$$\frac{\partial}{\partial t}|P\rangle = -H|P\rangle \,. \tag{1.1.5}$$

H operates on V. The Hamiltonian can be written as a sum of M nearest-neighbors terms plus two terms corresponding to the input and output of particles at the boundaries.

$$H \; = \sum_{i=1}^{M} H_{i,i+1} \, + \, h_1 \, + \, h_L \tag{1.1.6}$$

Here $M = L - 1$ for open and $M = L$ for periodic boundaries. [1] In the later case we consider only models in which h_1 and h_L vanish. H_i acts nontrivially locally on $V_i \otimes V_{i+1}$, and h_1 (h_L) on V_1 (V_L). Each of these operators can be represented in the spin basis as a $N^L \times N^L$ matrix:

$$\begin{aligned} H_i \; &= \sum_{\alpha,\beta=0}^{N-1} [\Gamma_{\alpha,\beta}\, E_i^{\alpha,\alpha} E_{i+1}^{\beta,\beta} - \sum_{\gamma,\delta=0}^{1} \Gamma_{\gamma,\delta}^{\alpha,\beta}\, E_i^{\gamma,\alpha} E_{i+1}^{\delta,\beta}\,]\,, \\ h_1 \; &= \sum_{\alpha,\beta=0}^{N-1} \Gamma_l^{\alpha,\beta} \Big(E_1^{\alpha,\alpha} \, - \, E_1^{\beta,\alpha} \Big) \end{aligned} \tag{1.1.7}$$

Here

$$E_i^{kl} \; = \; \mathbf{1}_1 \otimes \mathbf{1}_2 \otimes \cdots \otimes \mathbf{1}_{i-1} \otimes E^{kl} \otimes \mathbf{1}_{i+1} \cdots \otimes \mathbf{1}_L \tag{1.1.8}$$

where E^{kl} are $N \times N$ matrices with the entries $(E^{kl})_{nm} = \delta_{k,n}\delta_{l,m}$. The $N \times N$ identity matrix is denoted with $\mathbf{1}$. The definition of h_L is similar to the one of h_1 . The definition of the Hamiltonian ensures the conservation of probability. H has a bra ground state

$$\langle 0|H \; = \; 0 \tag{1.1.9}$$

which is the sum of all basis vectors

$$\langle 0| = \sum_{\{\beta\}} \langle \{\beta\}| \,. \tag{1.1.10}$$

[1] In order to avoid confusion in terminology we give in parenthesis an alternative denomination used in the literature: periodic boundary conditions (model on a ring), open boundary conditions (linear chain with closed ends), open boundary with particle input (chain with open ends).

The "vacuum" state $\langle 0|$, which can be represented in the spin basis as a line vector having all entries equal to 1, is an left eigenstate corresponding to eigenvalue 0 of the operators $H_{i,i+1}$, h_1 and h_L. Equation (1.1.7) with (1.1.4) states that the sum of the entries from each column of these matrices is 0. H has the same property (1.1.9). Note that the Hamiltonian is not necessarily hermitian.

The formal solution of (1.1.5) is:

$$|P(t)\rangle = \exp(-Ht)|P_0\rangle \tag{1.1.11}$$

where the initial state is denoted by $|P_0\rangle$ [2].

The expectation value of an operator X is given by the matrix element

$$< X > (|P_0\rangle, t) = \sum_{\{\beta\}} X(\{\beta\}) P(\{\beta\}; t) \; = \; \langle 0|X|P(t)\rangle \, . \tag{1.1.12}$$

The equation defining the time evolution of any observable can be easily derived with the help of (1.1.5):

$$\frac{\partial}{\partial t} < X > (|P_0\rangle, t) \; = \; -\langle 0|X H|P(t)\rangle \, . \tag{1.1.13}$$

Here X is the operator associated to that observable.

As an example we will write the equation giving the time evolution of the local particle concentration. The associated operator is giving the number of particles at site i

$$n_i \; = \; \mathbf{1}_1 \otimes \mathbf{1}_2 \otimes \cdots \otimes \mathbf{1}_{i-1} \otimes \frac{\mathbf{1} - \sigma^z}{2} \otimes \mathbf{1}_{i+1} \cdots \otimes \mathbf{1}_L . \tag{1.1.14}$$

Before we proceed we make an observation: finding a solution to (1.1.5) is equivalent with the knowledge of all the k-point equal-time correlation functions

$$\langle n_{i_1} \, n_{i_2} \cdots n_{i_k} \rangle (t) \; = \; \sum_{\{\beta\}} \beta_{i_1} \, \beta_{i_2} \cdots \beta_{i_k} P(\{\beta\}; t) \tag{1.1.15}$$

The set of definitions (1.1.15) corresponding to $k = 1, 2 \cdots L$ can be "inverted". The starting point is the obvious relation

$$P(\{\beta\}; t) \; = \; \sum_{\{\beta'\}} \langle \{\beta\} | \{\beta'\} \rangle \langle \{\beta'\} | P(t) \rangle$$

For variables β and β' having values 0 or 1 the Kronecker symbol $\delta_{\beta,\beta'}$ can be written as $2\beta\beta' - \beta - \beta' + 1$. After some computations one can show that

$$P(\{\beta\}; t) \; = \; \sum_S (-1)^G \cdot \langle \prod_{j \in S} n_j \; \rangle (t) \tag{1.1.16}$$

The sum is made after all subsets S of the set $\{ 1, 2 \cdots L \}$ which contain at least all the indices of the sites which are occupied in the configuration $\{\beta\}$, (i.e. $\forall \;\; S, \; \{ 1 \, \leq \, j \, \leq \, L \mid \beta_j \, = \, 1 \} \in S$). We denote with G the number of empty sites in the configuration $\{\beta\}$ having indices in S (i.e. $Q \, = \, \#i$ where $i \in S$ and $\beta_i \, = 0$). The equivalence mentioned before is thus proved.

We consider the coagulation-diffusion model with periodic boundaries and no particle input at the site 1 or L. Due to the nearest neighbor nature of the bulk reactions, from (1.1.14) and (1.1.13) one gets

$$\frac{\partial}{\partial t} \langle n_i \rangle (t) \; = \; - \, \langle n_i \, H_{i-1,i} \rangle \; - \; \langle n_i \, H_{i,i+1} \rangle \tag{1.1.17}$$

In the following we will skip the tensor products of identity matrices (1.1.8) appearing in the definition of the operators. In other words : we will represent $H_{i-1,i}$ as a $N^2 \times N^2$ matrices given by its nontrivial action on $V_{i-1} \otimes V_i$ and h_1 and h_L as $N \times N$ matrices. This will help us in writing the right side of (1.1.17) as a linear combination of one and to point functions. Let us take the first term. The operator n_i acts as the identity operator on V_{i-1} an as $\tilde{n} = (\mathbf{1} - \sigma^z)/2$ on V_i. We have:

$$- \left(\mathbf{1}_{i-1} \otimes \tilde{n}_i\right) H_{i-1,i} = \begin{pmatrix} 0 & 0 & 0 & 0 \\ 0 & 1 & 0 & 0 \\ 0 & 0 & 0 & 0 \\ 0 & 0 & 0 & 1 \end{pmatrix}_{i-1,i} \begin{pmatrix} 0 & 0 & 0 & 0 \\ 0 & -\Gamma_{10}^{01} & \Gamma_{01}^{10} & \Gamma_{01}^{11} \\ 0 & \Gamma_{10}^{01} & -\Gamma_{01}^{10} & \Gamma_{10}^{11} \\ 0 & 0 & 0 & -\Gamma_{01}^{11} - \Gamma_{10}^{11} \end{pmatrix}_{i-1,i}$$

In the definition of the expectation value the bra ground states is used. After multiplying the matrices appearing on the right side of (1.1) we use the obvious relations [13]

$$(1,1,1,1) \begin{pmatrix} 0 & 0 & 0 & 0 \\ 0 & -\Gamma_{10}^{01} & \Gamma_{01}^{10} & 0 \\ 0 & 0 & 0 & 0 \\ 0 & 0 & 0 & -\Gamma_{10}^{11} \end{pmatrix}_{i-1,i} = (1,1,1,1) \begin{pmatrix} 0 & 0 & 0 & 0 \\ 0 & -\Gamma_{10}^{01} & 0 & 0 \\ 0 & 0 & \Gamma_{01}^{10} & 0 \\ 0 & 0 & 0 & -\Gamma_{10}^{11} \end{pmatrix}_{i-1,i}$$

and

$$\alpha_1 \cdot \mathbf{1}_{i-1} \otimes \mathbf{1}_i + \alpha_2 \cdot \mathbf{1}_{i-1} \otimes \tilde{n}_i + \alpha_3 \cdot \tilde{n}_{i-1} \otimes \mathbf{1}_i + \alpha_4 \cdot \tilde{n}_{i-1} \otimes \tilde{n}_i =$$

$$\begin{pmatrix} \alpha_1 & 0 & 0 & 0 \\ 0 & \alpha_1+\alpha_2 & 0 & 0 \\ 0 & 0 & \alpha_1+\alpha_3 & 0 \\ 0 & 0 & 0 & \alpha_1+\alpha_2+\alpha_3+\alpha_4 \end{pmatrix}_{i-1,i} .$$

Thus one obtains

$$- \langle n_i H_{i-1,i} \rangle = -\Gamma_{10}^{01} \langle n_i \rangle(t) + \Gamma_{01}^{10} \langle n_{i-1} \rangle(t) + (\Gamma_{10}^{01} - \Gamma_{01}^{10} - \Gamma_{10}^{11}) \langle n_{i-1} n_i \rangle(t). \qquad (1.1.18)$$

Similarly one can express the second term on the right side of (1.1.17). The exact equation describing the dynamics of the one point function in the coagulation-diffusion model with periodic boundaries is

$$\frac{\partial}{\partial t} \langle n_i \rangle(t) = +\Gamma_{01}^{10} \langle n_{i-1} \rangle(t) - (\Gamma_{10}^{01} + \Gamma_{01}^{10}) \langle n_i \rangle(t) + \Gamma_{10}^{01} \langle n_{i+1} \rangle(t)$$

$$+ (\Gamma_{10}^{01} - \Gamma_{01}^{10} - \Gamma_{10}^{11}) \langle n_{i-1} n_i \rangle(t) + (\Gamma_{01}^{10} - \Gamma_{10}^{01} - \Gamma_{01}^{11}) \langle n_i n_{i+1} \rangle(t) \qquad (1.1.19)$$

Here i can take any value between 1 and L. The periodic boundary condition reads $n_{L+1} = n_1$.

For a general system, the time derivative of the one point function can be expressed as a linear combination of one and two point functions. Similarly, the time derivative of two point functions is a linear combination of one, two and three point functions. Only for some particular models the system of equations corresponding to the n point function (with $n = 1, 2, \cdots$) decouples from the higher order functions [28]. Thus, a exact solution giving the time dependence of the n point functions can not be given by integrating the equations mentioned above. In most of the cases one can study the systems only within the framework of the mean field approximation. The simplest way is to approximate the two point connected functions to be equal to 0:

$$\langle n_i n_j \rangle(t) \;=\; \langle n_i \rangle(t) \langle n_j \rangle(t) \tag{1.1.20}$$

In a periodic model, if the initial distribution $|P_0\rangle$ is translationally invariant than so is $|P(t)\rangle$ at all times t. This implies that the particle concentrations at all sites are equal

$$\langle n_i \rangle(t) \;=\; c(t), \quad \forall \;\; i.$$

Under this circumstances the mean field approximation (1.1.20) of (1.1.19) reads

$$\frac{\partial c}{\partial t} \;=\; -\left(\Gamma_{01}^{11} + \Gamma_{10}^{11}\right) c^2(t) \tag{1.1.21}$$

This implies that in the limit $t \longrightarrow \infty$ the particle concentration decays algebraically

$$c(t) \;\approx\; \left[\left(\Gamma_{01}^{11} + \Gamma_{10}^{11}\right) t\right]^{-1}$$

It is a well known fact that the long time behavior of the particle concentration in the coagulation model is algebraic in the thermodynamical limit [7, 2, 13]. However, the mean field result deduced above is not correct. In the exact solution the time exponent is $-\frac{1}{2}$. Also, in Chapter 4 we will give numerical evidence showing that for homogeneous noncorrelated initail conditions, the coefficient of the leading term is independent of the coagulation rates. The exact exponent can be obtained from (1.1.21) by making a supplementary approximation. One assumes that the sum of the coagulation rates must be replaced, in equation (1.1.19), by a "effective" rate which is proportional to the concentration

$$\Gamma_{01}^{11} + \Gamma_{10}^{11} \;=\; \zeta \, \langle n_i \rangle(t). \tag{1.1.22}$$

This implies that for $t \longrightarrow \infty, \quad c(t) \;\approx\; (2\,\zeta\, t)^{-1/2}$. It is interesting to remark that the same approximation as the one last mentioned was used in a slightly different context in [24]. It also has the effect of changing mean field equations in such a manner that they delivered a correct exponent. We will return to this point in Chapter 3.

Chapter 2

The Mean Field Description and the Phase Diagram of the Fully Asymmetric Exclusion Model

In this Chapter we give a full derivation of the mean field prediction for the one-dimensional fully asymmetric exclusion (FAE) model. We concentrate on the determination of the particle density profile and of the particle current in the steady state. With the help of these calculations a phase diagram can be derived. We present the results for two reasons. On the one hand, a complete mean field description is not given in the literature although the exact solution is known [17, 16, 18, 19]. On the other hand, we will be able to show that for at least two reaction - diffusion systems exhibiting boundary induced phase transitions, some features of the phase diagram are captured in the mean field description. One of them is the FAE model. The other one is the coagulation - diffusion system with particle input at the boundaries and will be discussed in Chapter 3. For both models many conclusions which can be drawn onhand of the mean field computations are validated by the exact solution.

The results of the calculations presented in this Chapter are applied in Ref. [29] for the mean field description of the CP-symmetry breaking, two species exclusion model.

The FAE model is easily defined. In the bulk the only process which is allowed is the hopping to the right of particles, if the rightmost neighboring site is empty (diffusion to the right). In addition, particles are allowed to entry the system at site 1 with rate α, and leave it at site L with rate β. We fix the time scale by choosing $\Gamma_{01}^{10} = 1$. The Hamiltonian H can be written as a sum of nearest-neighbor reaction matrices $H_{n,n+1}$ plus two further matrices for particle input h_L and output h_R:

$$H \;=\; h_1 \,+\, h_L \,+\, \sum_{n=1}^{L-1} H_{n,n+1}\,. \tag{2.0.1}$$

In the canonical basis of particle configurations ($|\emptyset\emptyset\rangle$, $|\emptyset A\rangle$, $|A\emptyset\rangle$, $|AA\rangle$) these matrices read

$$H_{n,n+1} \;=\; \begin{pmatrix} 0 & 0 & 0 & 0 \\ 0 & 0 & -1 & 0 \\ 0 & 0 & 1 & 0 \\ 0 & 0 & 0 & 0 \end{pmatrix}_{n,n+1} \tag{2.0.2}$$

and

$$h_1 = \begin{pmatrix} \alpha & 0 \\ -\alpha & 0 \end{pmatrix}_1 \qquad\qquad h_L = \begin{pmatrix} 0 & -\beta \\ 0 & \beta \end{pmatrix}_L . \tag{2.0.3}$$

The system possesses a symmetry. Adding (extracting) a particle at site 1 (L) is equivalent with extracting (adding) a hole at the same site. Whenever a particle jumps to the right, a hole jumps to the left. This means that the Hamiltonian H is invariant under the following transformation: a parity transformation (mirroring of the lattice around its middle-point) followed by the interchange of particles and holes and of the rates α and β.

The starting point of the computations are the exact equations describing the time evolution of the particle concentration $\langle n_i \rangle$. In the steady state one has (1.1.13):

$$\langle n_i H \rangle \ = 0 \quad i \ = \ 1, 2 \cdots L \tag{2.0.4}$$

For $1 \ < \ i \ < L$ we get:

$$\langle n_{i-1} \rangle \ - \ \langle n_{i-1} n_i \rangle \ = \ \langle n_i \rangle \ - \ \langle n_i n_{i+1} \rangle \tag{2.0.5}$$

For the FAE model one can define the particle current flowing between two neighboring sites i and $i+1$:

$$j_i = \sum_{\{\beta\}} \beta_i (1 - \beta_{i+1}) P(\{\beta\}, t) \ = \ \langle n_i (1 - n_{i+1}) \rangle \tag{2.0.6}$$

Equation (2.0.5) states that in the stationary state the current has a constant value along the lattice ($j_{i-1} \ = \ j_i$ for $i = 2, \cdots L-1$). This is a consequence of the pure diffusional nature of the bulk processes. We denote the value of the current with j. The boundary equations are obtained by taking $i = 1$ and $i = L$ in (2.0.4):

$$\langle n_1 \rangle \ = \ 1 - \frac{j}{\alpha} \tag{2.0.7}$$

$$\langle n_L \rangle \ = \ \frac{j}{\beta} \tag{2.0.8}$$

The particle-hole symmetry mentioned before is reflected in the fact that equations (2.0.5 - 2.0.8) are invariant under the transformation

$$\mathbf{1}_i \ - \ n_i \ \longrightarrow \ n_{L-i+1} \quad \text{and} \quad \alpha \ \longleftrightarrow \ \beta \tag{2.0.9}$$

2.1 The mean-field computations

Our goal is to compute the concentration profile $\langle n_i \rangle$ and the current j starting from (2.0.5 - 2.0.8). In these equations two point functions appear. In the following approximation we take the connected two point functions to be equal to 0, i.e:

$$\langle n_i n_j \rangle \ = \ \langle n_i \rangle \langle n_j \rangle \tag{2.1.1}$$

In general the fluctuations play an important role in the dynamics of one dimensional reaction-diffusion systems. We use the approximation (2.1.1) because we are interested in seeing what qualitative predictions one can obtain by using the mean field approach.

Using (2.1.1) the current conservation relation (2.0.5) becomes [16]:

$$\langle n_{i+1}\rangle \;=\; 1 \;-\; \frac{j}{\langle n_i\rangle} \tag{2.1.2}$$

These nonlinear equations together with the boundary conditions (2.0.7) and (2.0.8) define completely the mean field problem. This problem is difficult to solve. In Ref. [16] the values of the currents in the different phases are computed and a general description of the behavior of the density is given by analyzing the fixed points of relation (2.1.2).

Through our approach closed formulas for the particle density function are obtained. We are thus able to determine the nature (exponential or algebraic) of the decay of the density profile in the thermodynamical limit. This was done in [16] only in a particular case.

We take a continuum limit type of approach. First, by writing (2.1.2) for sites $i-1$ and i we get:

$$\langle n_i\rangle \;+\; \langle n_{i-1}\rangle \;-\; \langle n_i\rangle\langle n_{i-1}\rangle \;-\; \langle n_i\rangle\langle n_{i+1}\rangle \;=\; 2j \tag{2.1.3}$$

We replace the site index i with a coordinate x. We introduce the density function $\rho(x)$ defined in this chapter as the mean number of particles contained in an interval of length one centered around the point x. We also replace

$$\langle n_{i\pm1}\rangle \;=\; \rho(x) \;\pm\; \frac{d}{dx}\rho(x) \;+\; \frac{1}{2}\frac{d^2}{dx^2}\rho(x) \;+\cdots \tag{2.1.4}$$

By using this approach we lose the possibility to obtain a short distance description of the density profile. Nevertheless we are able to obtain interesting results concerning the asymptotic behavior of the concentration. We neglect all terms containing derivatives of order greater then one. Thus (2.1.3) together with (2.0.7) and (2.0.8) become:

$$2\rho(x) \;-\; \frac{d\rho(x)}{dx} \;-\; 2\rho^2(x) \;=\; 2j \tag{2.1.5}$$

$$\rho(0) \;=\; 1 \;-\; \frac{j}{\alpha} \tag{2.1.6}$$

$$\rho(L) \;=\; \frac{j}{\beta} \tag{2.1.7}$$

After separation of variables in (2.1.5) one gets:

$$\frac{(\frac{1}{4}-j)^{1/2}-\rho(x)+\frac{1}{2}}{\rho(x)-\frac{1}{2}+(\frac{1}{4}-j)^{1/2}} \;=\; K\; e^{-4(\frac{1}{4}-j)^{1/2}x} \tag{2.1.8}$$

The equations which determine the values of the constant K and the current j are obtained by using the boundary conditions (2.1.6)

$$K \;=\; \frac{(\frac{1}{4}-j)^{1/2}+\frac{j}{\alpha}-\frac{1}{2}}{(\frac{1}{4}-j)^{1/2}-\frac{j}{\alpha}+\frac{1}{2}} \tag{2.1.9}$$

and (2.1.7)

$$\frac{\left((\frac{1}{4}-j)^{1/2}-\frac{j}{\alpha}+\frac{1}{2}\right)\left((\frac{1}{4}-j)^{1/2}-\frac{j}{\beta}+\frac{1}{2}\right)}{\left((\frac{1}{4}-j)^{1/2}+\frac{j}{\alpha}-\frac{1}{2}\right)\left((\frac{1}{4}-j)^{1/2}+\frac{j}{\beta}-\frac{1}{2}\right)} \;=\; e^{-4(\frac{1}{4}-j)^{1/2}L}. \tag{2.1.10}$$

Relation (2.1.10) is an implicit equation which determines the particle current j as a function of the boundary rates α and β and of the size of the system L. It can not be solved explicitly for finite lattices.

However, we can determine the current j and the density (i.e. the value of K) as functions of α and β in the thermodynamical limit. *In this limit the maximal value which the current j can take is $\frac{1}{4}$*:

$$\lim_{L \longrightarrow \infty} j \ \leq \ \frac{1}{4}. \tag{2.1.11}$$

This can be proven with the help of equation (2.1.10):

Let us presume that the current can take values larger then $\frac{1}{4}$. This means that:

$$0 \ < \ \theta \ = \ (j - \frac{1}{4})^{1/2} \tag{2.1.12}$$

On the left and right side of (2.1.10) we have two phase factors:

$$\exp\Big(2\mathrm{i}(\theta_\alpha + \theta_\beta)\Big) \ = \ \exp(4\mathrm{i}\theta L) \tag{2.1.13}$$

Here we used the notation

$$\theta_u \ = \ \arctan\Big(\frac{4u\theta}{4\theta^2 + 2u - 1}\Big) \tag{2.1.14}$$

It follows from (2.1.13) that

$$\text{if } \exists \lim_{L \longrightarrow \infty} \theta \implies \exists \lim_{L \longrightarrow \infty} L\theta \tag{2.1.15}$$

and is finite. But this means that in the thermodynamical limit θ is zero which completes the proof of (2.1.11).

Before we start to present our result we notice that we have to cover only the half of the $\alpha\beta$ plane because of the particle-hole symmetry of the model (2.0.9)

$$\rho(x, \alpha, \beta) \ = \ 1 \ - \ \rho(L - x, \beta, \alpha) \tag{2.1.16}$$

This relation connects the particles density of any model with the holes density of the model in which the values of the input and output rates are permuted. The two densities are equal up to a reflection with respect to the middle-point of the lattice. Similarly one can show that the current of one model can be obtained from current of the other model by replacing $\alpha \leftrightarrow \beta$.

The case $j \ = \ 1/4$ is treated in subsection 2.1.3. In the subsections 2.1.1 and 2.1.2 the case in which the current is smaller than $\frac{1}{4}$ is treated. In this last case, both sides of (2.1.10) are equal to zero, in the thermodynamical limit, which implies

$$\Big(\sqrt{\frac{1}{4} - j} - \frac{j}{\beta} + \frac{1}{2}\Big)\Big(\sqrt{\frac{1}{4} - j} - \frac{j}{\alpha} + \frac{1}{2}\Big) \ = \ 0 \tag{2.1.17}$$

2.1.1 The high density phase

Lets see what happens if the first term of equation (2.1.17) cancels. We get [16]:

$$\jmath \ = \ \beta(1 - \beta) \ \text{ if } \ \beta \ < \ \frac{1}{2} \tag{2.1.18}$$

After computing the constant K, equation (2.1.8) reads

$$\rho(x) \;=\; \beta \,+\, (1-2\beta)\frac{(1-\beta)(\alpha-\beta)}{(1-\beta)(\alpha-\beta) \,-\, \beta(\alpha+\beta-1)\exp[-2(1-2\beta)x]} \tag{2.1.19}$$

Because the particle density is a positive defined function, one easily shows that (2.1.19) describes the density decay in the thermodynamical limit only if α is greater or equal to β (where, as noticed before, β is smaller than one half). In this case the system is in the so called "*high density phase*". This name is due to the fact that the particle density is almost constant in the bulk of the lattice where [16]:

$$\text{for} \quad x \gg 1, \;\; \rho(x) \approx 1-\beta > \frac{1}{2} \tag{2.1.20}$$

Near the left boundary the density decays exponentially from its initial value $\rho(0) = 1 - \beta(1-\beta)/\alpha$. The density is a decreasing (increasing) function of x if α is greater (smaller) than $1-\beta$. The characteristic length scale of the system is $(2-4\beta)^{-1}$.

2.1.2 The low density phase and the coexistence line

Using the particle hole symmetry (including relation 2.1.16) and the equations 2.1.18 - 2.1.20 one easily sees that if

$$\alpha < \frac{1}{2} \;\text{ and }\; \beta \geq \alpha \tag{2.1.21}$$

the current and the density are given by:

$$\mathrm{J} \;=\; \alpha(1-\alpha) \tag{2.1.22}$$

$$\rho(y) \;=\; 1 \,-\, \alpha \,-\, (1-2\alpha)\frac{(1-\alpha)(\beta-\alpha)}{(1-\alpha)(\beta-\alpha) \,-\, \alpha(\alpha+\beta-1)\exp[-2(1-2\alpha)y]} \tag{2.1.23}$$

Here we "moved" the origin of the reference frame to the right boundary i.e. we used the notation y for $L-x$. The values of the current (2.1.22) and of the density at the boundaries were also given in [16]. In this case the second term on the left side of equation (2.1.17) cancels.

The system is in the "low density phase". The particle density is almost constant far from the right boundary (i.e. for $y \gg 1$) where it has a value equal to α . Near the right boundary the density decays exponentially.

Equations (2.1.19), (2.1.22) and (2.1.23) show that for

$$\alpha \,+\, \beta \;=\; 1 \tag{2.1.24}$$

the density is constant along the system

$$\rho(x) \;=\; \alpha, \quad \forall x \tag{2.1.25}$$

This result is confirmed by the exact solution [16, 17, 18]. If (2.1.24) is satisfied the system is in a factorized state in which all connected correlation functions vanish

$$\langle n_i \rangle \;=\; \alpha \quad \forall \; i = 1, 2 \ldots L \tag{2.1.26}$$

$$\langle n_{i_1} n_{i_2} \ldots n_{i_k} \rangle \;=\; \langle n_{i_1} \rangle \langle n_{i_2} \rangle \ldots \langle n_{i_k} \rangle \quad \forall \; k \tag{2.1.27}$$

We have to complete the description in the case $\alpha = \beta < 1/2$. This is the so called "coexistence line" of the low and high density phases. Equations (2.1.19), (2.1.18) and (2.1.23) give the current and the behavior of the density near the boundaries [16]

$$j = \alpha(1-\alpha) \tag{2.1.28}$$
$$\lim_{x\to 0}\rho(x) = \alpha \tag{2.1.29}$$
$$\lim_{y\to 0}\rho(y) = 1-\alpha \tag{2.1.30}$$

The density is almost constant near the boundaries. We are interested in studying its behavior around the middle-point of the lattice. The density profile is symmetric with respect to a reflection about the $(\frac{L}{2},\frac{1}{2})$ point of the $x\rho$ plane (2.1.16)

$$\rho(x) = 1 - \rho(L-x) \tag{2.1.31}$$

We change again the origin of the reference frame, this time moving it in the middle-point of the lattice. We define

$$\tilde{\rho}(w) = \rho(x) - 1/2 \quad \text{where} \quad w = x - \frac{L}{2} \tag{2.1.32}$$

From (2.1.8 - 2.1.10) one gets

$$\tilde{\rho}(w) = (\alpha - \frac{1}{2})\tanh\Big((1/2-\alpha)w\Big), \tag{2.1.33}$$

which is, as expected, an uneven function of w.

In all the cases mentioned up to this point the decay of the density is exponential, which means that we have a characteristic length scale in the system namely

$$\lambda_u = \Big(2(1-2u)\Big)^{-1} \tag{2.1.34}$$

where $u=\beta$ in the high, and $u=\alpha$ in the low density phase, respectively.

2.1.3 The maximal current phase

The last case we have to analyze is the one in which, in the thermodynamical limit, the particle current is maximal

$$\lim_{L\longrightarrow\infty} j(\alpha,\beta,L) = \frac{1}{4}. \tag{2.1.35}$$

The first step is to find a solution to (2.1.10) in the first order of an expansion in powers of $\frac{1}{L}$. We make the ansatz:

$$(\frac{1}{4} - j)^{1/2} = \frac{a}{L^u} + O\Big(\frac{1}{L^v}\Big) \quad \text{where} \quad v > u \tag{2.1.36}$$

From a Taylor expansion of (2.1.10) one gets $u = 1$ and $a = \frac{\mathrm{i}\pi}{2}$. Thus:

$$j = \frac{1}{4} + \frac{\pi^2}{4L^2} + O\Big(\frac{1}{L^v}\Big) \quad \text{where} \quad v > 2 \tag{2.1.37}$$

By using (2.1.37) in (2.1.10) one gets

$$\rho(x) = \frac{1}{2} + \frac{1}{L}\frac{\pi}{2}\cot\Big(\frac{\pi x}{L}\Big) - \frac{1}{L^2}\frac{\pi^2\alpha}{(2\alpha-1)}\Big[1 + \cot^2\Big(\frac{\pi x}{L}\Big)\Big] + O\Big(\frac{1}{L^3}\Big) \tag{2.1.38}$$

This result, up to the term proportional to $\frac{1}{L^2}$, is confirmed in [16].

The value of the density far from the ends of the lattice is almost constant and equal to $\frac{1}{2}$. In the maximal current phase $\rho(x)$ is a monotonically decreasing function of x (see 2.1.5). Thus from the fact that $\rho(0) \leq 0.5 \leq \rho(L)$ and from equations (2.1.6) and (2.1.7) we get the conditions which define the domain of the maximal current phase

$$\alpha > \frac{1}{2} \quad \text{and} \quad \beta > \frac{1}{2} \tag{2.1.39}$$

We have thus covered the whole $\alpha\beta$ plane. In the thermodynamical limit the particle density function decays algebraically towards the bulk value

$$\rho(x) - \frac{1}{2} = \frac{1}{2x} - \frac{\alpha}{x^2\,(2\alpha - 1)} \tag{2.1.40}$$

The leading term is of order $\frac{1}{x}$ and its coefficient is independent of the rates of the boundary processes. With the help of (2.1.16) we can write the relation describing the decay of the density near the right boundary. All we have to do is to replace α with β, x with y and to reverse the signs of the two left terms of (2.1.40).

Equation (2.1.38) leads us to the important conclusion that the particle density function scales in the limit

$$L \to \infty,\ x \to \infty \quad \text{with} \quad z = \frac{x}{L} \ \text{fixed.} \tag{2.1.41}$$

The scaling relation is

$$\lim_{\substack{L \to \infty \\ x \to \infty \\ z=\frac{x}{L}\ fixed}} L^{\delta} \left(\rho(x) - \frac{1}{2}\right) = \frac{\pi}{2} \cot(\pi z) \tag{2.1.42}$$

The scaling exponent δ is 1. The scaling function is independent of the input and output rates. In chapter 3 we give an example of system for which the scaling behavior is nontrivial and the scaling function can be computed exactly.

2.2 The phase diagram. Exact and mean field results

In this section we summarize the results of the mean field computations and compare them with the exact solution of the one-dimensional fully asymmetric model.

The complete phase diagram is given in Figure 2.1. A first criterion in defining a phase is the dependence of the current j on α and β. The capital letters $\mathbf{A}, \mathbf{B}, \mathbf{C}$ stand for the different values of the current

$$\begin{aligned}
\text{Phase } \mathbf{A} : \ j &= \beta(1-\beta) \quad \text{for } \beta < \frac{1}{2},\ \alpha > \beta \\
\text{Phase } \mathbf{B} : \ j &= \alpha(1-\alpha) \quad \text{for } \alpha < \frac{1}{2},\ \beta > \alpha \\
\text{Phase } \mathbf{C} : \ j &= \frac{1}{4} \qquad\qquad \text{for } \alpha > \frac{1}{2},\ \beta > \frac{1}{2}
\end{aligned} \tag{2.2.1}$$

The dependence of the current on the boundary rates was first deduced in the mean field approximation in Ref. [16]. Region $\mathbf{A}$ ($\mathbf{B}$) corresponds to the high (low) density phase and region $\mathbf{C}$

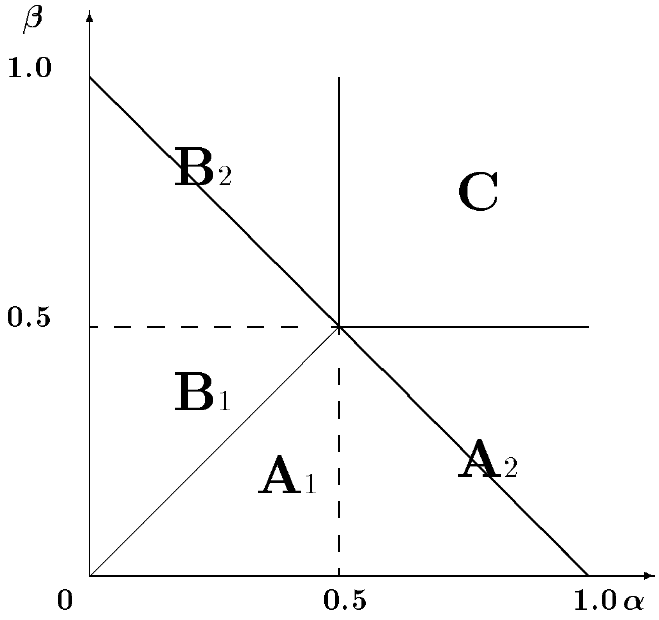

Figure 2.1: Phase diagram of the fully asymmetric exclusion model. The dashed lines come from the exact solution. The thick line ($\alpha + \beta = 1$) corresponds to the factorized states.

is the maximal current phase. The same dependence (2.2.1) was obtained within the exact solution [17, 18]. The mean field predictions concerning the values of the particle density at the two endpoints of the lattice are thus also confirmed (these values are obtained from Equations (2.0.7) and (2.0.8)).

For the high (low) density phase, the exact results confirm the mean field description: the density function is almost constant along the lattice with the exception of the "tail" at the left (right) boundary. The "plateau" values (see 2.1.20) $1-\beta$ and α respectively, are confirmed. The decay of the density to its bulk value is exponential.

Because the two phases (**A** and **B**) are connected by the particle-hole symmetry of the model, we discuss in the following only the high density phase. The "tail" of the density profile is indeed a decreasing function of i if $\alpha > 1-\beta$ and is increasing in the opposite case [18]. If $\alpha = 1-\beta$ the system is in a factorized state with constant density function and no correlations, irrespective of the lattice length. Up to this point, the mean field predictions are confirmed.

In the following we reproduce the exact results as they are given in Ref. [17] and [18]. The formulae give the particle concentration decay near the boundaries for $i \gg 1$. This corresponds to the behavior of the density at very small scaling argument $z \to 0$. The series are truncated after the leading terms.

The dependence of the correlation length on the boundary rates as it was obtained in the mean field approach (2.1.34) is not correct, as will be shown in the sequel.

For $\underline{\beta < \alpha < 1/2}$, (corresponding to the region $\mathbf{A}_1$ in the phase diagram) the particle density is given by

$$\langle n_i \rangle = (1-\beta) - (1-2\alpha)\left(\frac{\beta(1-\beta)}{\alpha(1-\alpha)}\right)^i \tag{2.2.2}$$

We see that instead of the mean field prediction λ_β, , the characteristic length scale in the system is equal with the difference of two correlation lengths [18]

$$\zeta^{-1} \;=\; \zeta_\beta^{-1} \;-\; \zeta_\alpha^{-1}; \qquad \text{where} \quad \zeta_\sigma^{-1} \;=\; -\log[4\sigma(1-\sigma)] \tag{2.2.3}$$

In the mean field approach, on the coexistence line ($\alpha = \beta < \frac{1}{2}$) the system is characterized by a common, nonvanishing, length scale ($\lambda_\alpha \;=\; \lambda_\beta$). The mean field prediction for the density function (2.1.33) vanishes in the scaling limit (2.1.41). The exact solution shows that in this case the specific length ζ diverges. The density profile varies linearly from α (at the left endpoint) to $1-\alpha$ (at the right endpoint) of the system.

$$\langle n_i \rangle = \alpha + \frac{i}{L}(1-2\alpha). \tag{2.2.4}$$

On the coexistence line the behavior of the density in the scaling limit is nontrivial. The scaling exponent is 0 and the scaling function is linear in z.

If α approaches the value 1/2 from below, the correlation length ζ_α diverges. In the region $\mathbf{A}_2$ of the phase diagram ($\beta < 1/2 < \alpha$) the particle density function is given by

$$\langle n_i \rangle = (1-\beta) - \frac{4^{i-1}(\beta(1-\beta))^i}{\sqrt{\pi} i^{\frac{3}{2}}}\left(\frac{1}{(1-2\alpha)^2} - \frac{1}{(1-2\beta)^2}\right) \tag{2.2.5}$$

The dependence on i is more complicated than the one in (2.2.2). The decay of the density is still dominated by the exponential factor but an algebraic factor $\propto\; i^{-3/2}$ is also present.

If now, in addition, β approaches the value $\frac{1}{2}$ the correlation length ζ_α and thus ζ diverge. If both α and β are greater than one half the system is in the maximal current phase (denoted by $\mathbf{C}$ in the phase diagram). The bulk value of the density is $\frac{1}{2}$. The decay of the particle density towards this value is algebraic.

$$\langle n_i \rangle = \frac{1}{2} + (1-\delta_{2\alpha,1})\frac{1}{2\sqrt{\pi} i^{\frac{1}{2}}} \tag{2.2.6}$$

The exponent of the leading term in the $\frac{1}{i}$ expansion is 1/2, not 1 as predicted in the mean field computation (2.1.40). Its coefficient is independent of the boundary rates. No exact result concerning the behavior of the density function in the scaling limit in this phase is known. For a detailed discussion of the phase diagram see Ref. [18].

Chapter 3

The One-Dimensional Coagulation-Diffusion Model with External Particle Input

The coagulation model studied in this chapter is defined as follows [1]. Particles of one species diffuse stochastically on a linear one-dimensional lattice with L sites. The diffusion may be biased due to some external force. If two particles meet at the same site, they coalesce to a single one. In addition particles are added stochastically at a given rate at the endpoints of the lattice. Altogether the dynamics is defined by the four nearest neighbor and two one-site processes which are shown in Figure 3.1.

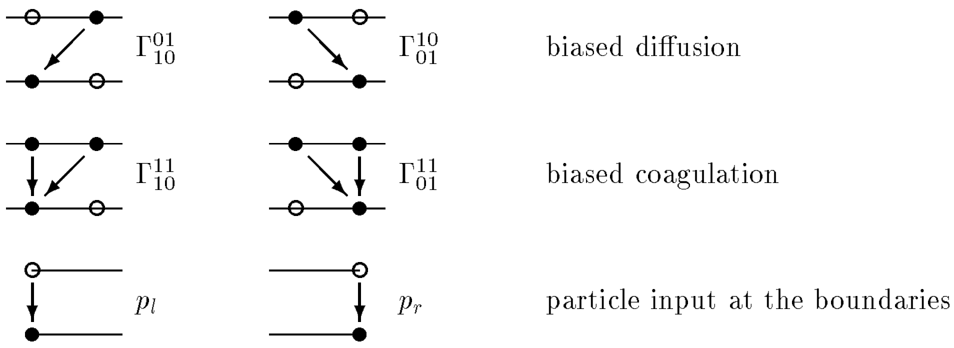

Figure 3.1: Bulk and boundary processes in the coagulation-diffusion model

The Hamiltonian H (1.1.5) can be written as a sum of nearest-neighbor reaction matrices $H_{n,n+1}$ plus two further matrices for particle input h_1 and h_l:

$$H \;=\; h_1 + h_L + \sum_{n=1}^{L-1} H_{n,n+1}\,. \tag{3.0.1}$$

[1] This Chapter is entirely based on Ref. [26].

In the canonical basis of particle configurations ($|\emptyset\emptyset\rangle$, $|\emptyset A\rangle$, $|A\emptyset\rangle$, $|AA\rangle$) these matrices read

$$H_{n,n+1} \;=\; \left(\begin{array}{cccc} 0 & 0 & 0 & 0 \\ 0 & \Gamma^{01}_{10} & -\Gamma^{10}_{01} & -\Gamma^{11}_{01} \\ 0 & -\Gamma^{01}_{10} & \Gamma^{10}_{01} & -\Gamma^{11}_{10} \\ 0 & 0 & 0 & \Gamma^{11}_{10}+\Gamma^{11}_{01} \end{array} \right)_{n,n+1} \tag{3.0.2}$$

and

$$h_1 \;=\; \left(\begin{array}{cc} p_l & 0 \\ -p_l & 0 \end{array} \right)_1 \qquad\qquad h_L \;=\; \left(\begin{array}{cc} p_r & 0 \\ -p_r & 0 \end{array} \right)_L . \tag{3.0.3}$$

It is useful to introduce some notations

$$r \;=\; \frac{2\,(\Gamma^{10}_{01}-\Gamma^{01}_{10})}{(\Gamma^{10}_{01}+\Gamma^{01}_{10})}, \qquad s \;=\; \frac{2\,(\Gamma^{11}_{01}+\Gamma^{11}_{10})}{(\Gamma^{10}_{01}+\Gamma^{01}_{10})}, \qquad t \;=\; \frac{2\,(\Gamma^{11}_{01}-\Gamma^{11}_{10})}{(\Gamma^{10}_{01}+\Gamma^{01}_{10})}, \qquad q \;=\; \left(\frac{\Gamma^{10}_{01}}{\Gamma^{01}_{10}}\right)^{1/2} \tag{3.0.4}$$

$c(i)$ denotes the particle concentration at the site i. When we will consider the continuum limit (the lattice spacing $\lambda \to 0$), we will use the notation

$$\rho(x) \;=\; \lambda^{-1} c\left(\frac{i}{\lambda}\right), \qquad \hat{r} \;=\; \frac{r}{\lambda}, \qquad \hat{s} \;=\; \frac{s}{\lambda}, \qquad \hat{p} \;=\; \frac{p_l}{\lambda^2} \tag{3.0.5}$$

Let us take a look at the mean field description of the model. In the stationary state the set of discrete equations is

$$\begin{aligned} 0 \;&=\; \Gamma^{10}_{01}\langle n_{j-1}\rangle \;+\; \Gamma^{01}_{10}\langle n_{j+1}\rangle \;-\; (\Gamma^{01}_{10}+\Gamma^{10}_{01})\,\langle n_j\rangle \\ &\quad +(\Gamma^{01}_{10}-\Gamma^{10}_{01}-\Gamma^{11}_{10})\,\langle n_{j-1}\rangle\,\langle n_j\rangle \;+\; (\Gamma^{10}_{01}-\Gamma^{01}_{10}-\Gamma^{11}_{01})\,\langle n_j\rangle\,\langle n_{j+1}\rangle \qquad (1<j<L) \\ 0 \;&=\; p_l \;-\; (p_l+\Gamma^{10}_{01})\,\langle n_1\rangle \;+\; \Gamma^{01}_{10}\,\langle n_2\rangle \;+\; (\Gamma^{10}_{01}-\Gamma^{01}_{10}-\Gamma^{11}_{01})\,\langle n_1\rangle\,\langle n_2\rangle \\ 0 \;&=\; p_r-(p_r+\Gamma^{01}_{10})\langle n_L\rangle+\Gamma^{10}_{01}\,\langle n_{L-1}\rangle \;+\; (\Gamma^{01}_{10}-\Gamma^{10}_{01}-\Gamma^{11}_{10})\,\langle n_{L-1}\rangle\,\langle n_L\rangle \end{aligned} \tag{3.0.6}$$

Here $\langle n_j\rangle$ denotes the local particle density in the stationary state at site j. In the continuum limit the bulk equation becomes

$$\frac{d^2}{dx^2}\rho(x) - \hat{r}\frac{d}{dx}\rho(x) - \hat{s}\,\rho^2(x) \;=\; 0 \tag{3.0.7}$$

For a system with particle input only at the left boundary of the system, the asymptotic solutions for large x turn out to be

$$\begin{array}{lll} \hat{r}<0 & \text{(bias to the left) :} & n(x) \propto e^{-|\hat{r}|x} \\ \hat{r}=0 & \text{(symmetric diffusion) :} & n(x) \sim \frac{6}{\hat{s}\,x^2} \\ \hat{r}>0 & \text{(bias to the right) :} & n(x) \sim \frac{\hat{r}}{\hat{s}\,x} \end{array} \tag{3.0.8}$$

The mean field approximation predicts an algebraic decay of the concentration profile for $\hat{r} \geq 0$. This profile is universal in the sense that its asymptotic behavior does not depend on the input rate p_l. For $\hat{r}<0$ the concentration decays exponentially. These qualitative results are confirmed by the exact solution (3.0.11-3.0.15).

The predicted exponents are -2 for symmetric diffusion and -1 for biased diffusion away from the input source. They differ from the correct exponents -1 and $-\frac{1}{2}$ by a factor of two [24]. The value of the correlation legth, in the case of biased diffusion to the left, turns out to be $4\log(q)$ and not $|\hat{r}|$.

These conclusions are perfectly similar with the ones derived for the fully asymmetric exclusion model in Chapter 2. We have thus two examples of systems for which the mean field equation describe correctly the phase diagram and the nature (exponential or algebraic) of the decay of the density. In both cases the correlation lengthes for the massive, respectively the exponents for the massless phases differ from the correct ones.

The reason is that in the mean field approach one neglects any correlations of the particles. The correct exponents can be obtained through improved mean field calculations [24]. Assuming that the coagulation rate $\hat{s}$ is proportional to the concentration $\hat{s} = \zeta\rho(x)$, the densities become

$$\begin{array}{lll} q < 1 & \text{(bias to the left)}: & \rho(x) \propto e^{-|\hat{r}|x} \\ q = 1 & \text{(symmetric diffusion)}: & \rho(x) \approx \sqrt{\frac{2}{\zeta}}\, x^{-1} \\ q > 1 & \text{(bias to the right)}: & \rho(x) \approx \sqrt{\frac{\hat{r}}{2\zeta}}\, x^{-1/2} \end{array} \tag{3.0.9}$$

The exponents in the algebraic fall-off, for $q \geq 1$, as they are given above are the same with the ones from the exact solution. The same assumption (1.1.22) delivers the correct exponent in the case of the asymptotic time behavior of the mean concentration in the coagulation model with periodic boundaries.

As mentioned in the Introduction, the model is exactly solvable by means of the IPDF method for a special choice of the rates. The IPDF method is applicable if

$$\Gamma_{01}^{10} = \Gamma_{01}^{11} = q\,, \qquad \Gamma_{10}^{01} = \Gamma_{10}^{11} = q^{-1}\,. \tag{3.0.10}$$

These conditions are equivalent to $r = t$ and $s = 2$. This will also be called the fermionic case (the Hamiltonian can be diagonalized in terms of free fermions [15, 13, 30]). The special case $q = 1$, $p_r = p_l = \infty$ was already studied in a paper by Derrida et al [31] which was a source of inspiration for the present work. We list now our main results in the $p_r = 0$ case:

a) *Lattice in the thermodynamical limit* (j fixed, $L \to \infty$)

$$c(j) = \frac{2}{\pi j} + \frac{1}{\pi j^2} - \frac{1}{2\pi j^4} + \left(\frac{3}{8\pi} - \frac{12}{\pi p_l^2}\right)\frac{1}{j^5} + O(j^{-6}) \qquad q = 1 \tag{3.0.11}$$

$$c(j) = \sqrt{\frac{q^2-1}{(q^2+1)\pi j}}\left[1 + \left(\frac{3q^4+20q^2-1}{8(q^4-1)} - \frac{(q^2-1)^3}{2q^2(q^2+1)p_l^2}\right)\frac{1}{j}\right] + O(j^{-5/2}) \qquad q > 1 \tag{3.0.12}$$

$$c(j) = q^{4j}\left(\sqrt{\frac{1-q^2}{(q^2+1)\pi j}} + O(j^{-3/2})\right) \qquad q < 1 \tag{3.0.13}$$

Several exact values for $c(j)$ are given in Appendix A.

b) *Continuum and thermodynamical limit* (x fixed, $L \to \infty$)

$$\rho(x) \;=\; \frac{2}{\pi x} - \frac{12}{\pi \hat{p}^2 x^5} + \frac{5040}{\pi \hat{p}^4 x^9} + O(\hat{p}^{-6} x^{-13}) \qquad q = 1 \qquad (3.0.14)$$

$$\rho(x) \;=\; \sqrt{\frac{\hat{r}}{2\pi x}} + \frac{1}{4\sqrt{2\pi \hat{r}}}\left[\frac{11}{2} - \frac{\hat{r}^4}{\hat{p}^2}\right]\frac{1}{x^{3/2}} \;+\; O(x^{-5/2}) \qquad q > 1 \qquad (3.0.15)$$

c) *Continuum and scaling limit* ($z = \frac{x}{L}$ fixed, $L \to \infty,\ q = 1$)

$$\lim_{\substack{L\to\infty \\ x\to\infty \\ z=\frac{x}{L}\ \text{fixed}}} \; L\,\rho(x) \;=\; \Phi(z) \qquad (3.0.16)$$

$$\Phi(z) \;=\; \frac{\sinh(\pi z) \,+\, \sin(\pi z)}{\cosh(\pi z) \,-\, \cos(\pi z)} \;+\; \sum_{k=1}^{+\infty}\left\{\frac{\sinh(2\pi(z/2-k)) \,+\, \sin(\pi z)}{\cosh(2\pi(z/2-k)) \,-\, \cos(\pi z)} \;+\; (\; k \;\longleftrightarrow\; -k \;)\right\} \qquad (3.0.17)$$

As a by-product, the one-hole functions are also obtained. This result is not trivial since they represent two-point correlation functions.

In the long Section 3.1 and in the Appendices A and B these results are derived. Many of our calculations are extensions of results obtained in references [13] and [30] from which we borrow the notations. Also in Section 3.1 we give the spectrum of the Hamiltonian in the one-hole sector. For $q \neq 1$ the spectrum is massive in spite of the algebraic behavior seen in Eqs. (3.0.12) and (3.0.15). For $q = 1$ most of the excitations are massless (they coincide with those of the open chain ($p_l = 0$)) but there are also some massive excitations with a mass given by p_l. In many systems time-like and space-like properties seem to be coupled in the sense that long range correlations in time imply long range correlations in space. This is not necessary valid for stochastic models which are not isotropic. As we will see in this model one can have short range correlations in time but long range correlations in space (for another example, see Ref. [2]).

In Section 3.2 we consider the problem of the universality: The coefficient $\frac{2}{\pi}$ for the leading contribution in the $q = 1$ case (see Eqs. (3.0.11) and (3.0.14)), the coefficient $\sqrt{\frac{q^2-1}{(q^2+1)\pi}}$ for $q > 1$ (see Eqs. (3.0.12) and (3.0.15)) and the finite-size scaling function (3.0.17). For this purpose we keep the definition $\sqrt{\frac{\Gamma^{10}_{01}}{\Gamma^{01}_{10}}} = q$ but leave the coagulation rates Γ^{11}_{01} and Γ^{11}_{10} arbitrary. For the open chain (no input) the spectra are known to be massless for $q = 1$ and massive for $q > 1$ [2]. The modifications introduced by the boundary terms are supposed not to change radically the picture. Using Monte Carlo simulations (the details are given in Appendix C) we show that indeed for several values of Γ^{11}_{10} and Γ^{11}_{01} the expansion coefficients as well as the finite-size scaling functions are universal.

3.1 Exact solution in the $\Gamma^{10}_{01} = \Gamma^{11}_{01} = q$, $\Gamma^{01}_{10} = \Gamma^{11}_{10} = q^{-1}$ case.

3.1.1 Finite lattice calculations

In this Section we give the full solution of the coagulation model with particle input at the boundaries. We use the IPDF formalism [8]-[12] in which the whole problem is formulated in terms of probabilities for finding sequences of unoccupied sites (holes). In this basis the master equation leads to a hierarchy of sets of equations according the number of holes. It is known [15] that these sets decouple from the higher ones provided that the rates for diffusion and coagulation coincide (see Eq. (3.0.10)). Therefore the one-hole sector decouples from the higher sectors and can be solved separately. In what follows we will assume that the above condition holds.

For completeness we will consider the model with input at the left end (rate p_l) and right end (rate p_r). We will actually show that by solving the problem with $p_r = 0$ one can obtain the general solution $p_r \neq 0$. Although in principle feasible, we didn't look to the case when one has also output of particles at both end.

Although not obviously needed for the study of the stationary state, we will also give the spectrum of the problem in the one-hole sector for two reasons. One is technical: the eigenfunctions and eigenvalues occur in the expression of the stationary state hole probabilities. The second one is related to the physical significance of our result: it is important to know whether one has massless or massive excitations.

Let $\Omega(j,m,t)$ denote the probability to find the sites $j+1, j+2, \dots m$ empty at time t. By a careful analysis of the elementary processes taking place at the edges of the hole one is led to the following equations of motion for the one-hole sector:

- for holes which do not touch the boundaries ($0 < j < m < L$):

$$\begin{aligned} \frac{d}{dt}\Omega(j,m,t) &= q\,\Omega(j-1,m,t) + q^{-1}\,\Omega(j+1,m,t) \\ &\quad + q\,\Omega(j,m-1,t) + q^{-1}\,\Omega(j,m+1,t) - 2\,(q+q^{-1})\,\Omega(j,m,t) \end{aligned} \tag{3.1.1}$$

- for holes touching the left boundary ($0 = j < m < L$):

$$\frac{d}{dt}\Omega(0,m,t) = q\,\Omega(0,m-1,t) + q^{-1}\,\Omega(0,m+1,t) - (q+q^{-1}+p_l)\,\Omega(0,m,t) \tag{3.1.2}$$

- for holes touching the right boundary ($0 < j < m = L$):

$$\frac{d}{dt}\Omega(j,L,t) = q\Omega(j-1,L,t) + q^{-1}\Omega(j+1,L,t) - (q+q^{-1}+p_r)\,\Omega(j,L,t) \tag{3.1.3}$$

- for the hole extending over the whole chain ($j = 0, m = L$):

$$\frac{d}{dt}\Omega(0,L,t) = -(p_l+p_r)\,\Omega(0,L,t)\,. \tag{3.1.4}$$

In these equations we have taken $\Omega(j,j,t) = 1$. This leads to an *inhomogeneous* system of equations. Separating the time dependence and introducing rescaled probabilities

$$\Omega(j,m,t) = e^{-\Lambda t} q^{+j+m}\,\tilde{\Omega}(j,m) \tag{3.1.5}$$

we obtain the simplified system of equations

$$\begin{aligned} \Big(2(q+q^{-1}) - \Lambda\Big)\tilde{\Omega}(j,m) &= \tilde{\Omega}(j-1,m) + \tilde{\Omega}(j+1,m) + \tilde{\Omega}(j,m-1) + \tilde{\Omega}(j,m+1) && (3.1.6)\\ \Big(q+q^{-1}+p_l-\Lambda\Big)\,\tilde{\Omega}(0,m) &= \tilde{\Omega}(0,m-1) + \tilde{\Omega}(0,m+1) && (3.1.7)\\ \Big(q+q^{-1}+p_r-\Lambda\Big)\,\tilde{\Omega}(j,L) &= \tilde{\Omega}(j+1,L) + \tilde{\Omega}(j-1,L) && (3.1.8)\\ \Big(p_l+p_r-\Lambda\Big)\,\tilde{\Omega}(0,L) &= 0 && (3.1.9) \end{aligned}$$

with the inhomogeneous boundary condition $\tilde{\Omega}(j,j) = q^{-2j}$.

The *homogeneous* set of solutions describes the relaxational modes of the system. It is obtained by setting $\tilde{\Omega}(j,j)=0$ and can be computed easily by using similar techniques as in Ref. [13] which rely mainly on the invariance of the bulk equation (3.1.1) under reflections $j \leftrightarrow m$ and $j \leftrightarrow L-m$. Denoting

$$g(j,z) \;=\; \frac{\sinh\Big(j\,\mathrm{arcsinh}\frac{1}{2}(q+q^{-1}-z)\Big)}{\sinh\Big(L\,\mathrm{arcsinh}\frac{1}{2}(q+q^{-1}-z)\Big)} \tag{3.1.10}$$

the homogeneous solutions are

$$\begin{aligned}
\Phi_0(j,m) &= g(L-j,p_l)\,g(m,p_r) - g(L-m,p_l)\,g(j,p_r) && (3.1.11)\\
\Phi_k^{(L)}(j,m) &= \sin\frac{\pi kj}{L}\,g(L-m,p_l) - \sin\frac{\pi km}{L}\,g(L-j,p_l) && (3.1.12)\\
\Phi_k^{(R)}(j,m) &= \sin\frac{\pi kj}{L}\,g(m,p_r) - \sin\frac{\pi km}{L}\,g(j,p_r) && (3.1.13)\\
\Phi_{k,l}(j,m) &= \sin\frac{\pi kj}{L}\,\sin\frac{\pi lm}{L} - \sin\frac{\pi km}{L}\,\sin\frac{\pi lj}{L}\,. && (3.1.14)
\end{aligned}$$

They have the excitation energies

$$\begin{aligned}
\Lambda_0 &= p_l + p_r && (3.1.15)\\
\Lambda_k^{(L)} &= q+q^{-1}+p_l-2\cos\frac{\pi k}{L} && (3.1.16)\\
\Lambda_k^{(R)} &= q+q^{-1}+p_r-2\cos\frac{\pi k}{L} && (3.1.17)\\
\Lambda_{k,l} &= 2(q+q^{-1}) - 2\cos\frac{\pi k}{L} - 2\cos\frac{\pi l}{L} && (3.1.18)
\end{aligned}$$

where $1 \le k < l \le L$. In contrast to the coagulation model without particle input ($p_r = p_l = 0$) where the spectrum is massless for $q=1$ and massive otherwise (q real), in the case of particle input, the spectrum is more complex. Even for $q=1$ where most of the excitations are massless (Eq.(3.1.18)) we get some massive ones too (Eqs.(3.1.15) - (3.1.17)).

The derivation of the *inhomogeneous* (steady state) solution is more difficult. For symmetric coagulation on a ring with infinite particle input at a single site an exact solution has been found recently in Refs. [31, 32]. This solution applies to an open chain with symmetric diffusion (q=1) and infinite particle input at both ends ($p_l = p_r = \infty$). It is given by $\tilde{\Omega}(j,j)=1$ and

$$\tilde{\Omega}(j,m) = \frac{8}{L^2}{\sum_{k,l=1}^{L-1}}' \frac{\sin\frac{\pi k}{L}\sin\frac{\pi l}{L}\,(\sin\frac{\pi kj}{L}\sin\frac{\pi lm}{L} - \sin\frac{\pi km}{L}\sin\frac{\pi lj}{L})}{(\cos\frac{\pi l}{L}-\cos\frac{\pi k}{L})(2-\cos\frac{\pi k}{L}-\cos\frac{\pi l}{L})} \qquad (j<m) \tag{3.1.19}$$

where the prime indicates that the sum runs only over even values of k and odd values of l. Formally this solution can be expressed in terms of the two-particle excitations (3.1.14) by

$$\tilde{\Omega}(j,m) \;=\; \frac{8}{L^2}\sum_{k,l=1}^{L-1}\frac{f_{k,l}\,\Phi_{k,l}(j,m)}{\Lambda_{k,l}} \tag{3.1.20}$$

where

$$f_{k,l} \;=\; \frac{1}{2}\,(1-(-)^{k+l})\,\frac{\sin\frac{\pi k}{L}\sin\frac{\pi l}{L}}{\cos\frac{\pi l}{L}-\cos\frac{\pi k}{L}}\,. \tag{3.1.21}$$

plays the role of a structure function. However, we one can prove that the general stationary solution for the asymmetric diffusion and finite particle input rates has the same structure and differs only in the structure function $f_{k,l}$. This function can be derived as follows. Let us symbolize a contraction of two functions over momentum indices k,l by $\langle\cdot,\cdot\rangle_{k,l}$ and similarly a contraction over spatial indices by $\langle\cdot,\cdot\rangle_{j,m}$. Then Eq. (3.1.20) reads $\tilde{\Omega} = \langle f, \frac{\Phi}{\Lambda}\rangle_{k,l}$ and therefore the application of the discretized Laplacian $\Delta\Phi = \Lambda\Phi$ yields $\Delta\tilde{\Omega} = \langle f,\Phi\rangle_{k,l}$ which is zero everywhere except at the boundaries. Using the orthogonality relation $\langle\Phi_{k,l},\Phi_{k',l'}\rangle_{j,m} \sim \delta_{k,k'}\delta_{l,l'}$ one can therefore compute f by

$$f \sim \langle f,\delta\delta\rangle_{k,l} \sim \langle f,\langle\Phi,\Phi\rangle_{j,m}\rangle_{k,l} \sim \langle\langle f,\Phi\rangle_{k,l},\Phi\rangle_{j,m} \sim \langle\Delta\tilde{\Omega},\Phi\rangle_{j,m}\,. \tag{3.1.22}$$

Carrying out these contractions it turns out that the structure function f consists of three parts

$$f_{k,l} \;=\; f^{(\infty)}_{k,l} \;+\; f^{(L)}_{k,l} \;+\; f^{(R)}_{k,l}\,. \tag{3.1.23}$$

The first part $f^{(\infty)}_{k,l}$ describes the asymmetric coagulation model with infinite particle input rates at *both* ends. It is given by

$$f^{(\infty)}_{k,l} \;=\; (1-(-)^{k+l}q^{-2L})\,\frac{(q+q^{-1})^2\,\sin\frac{\pi k}{L}\sin\frac{\pi l}{L}\sin\frac{\pi(k+l)}{2L}\sin\frac{\pi(k-l)}{2L}}{(q^2+q^{-2}-2\cos\frac{\pi(k+l)}{L})\,(q^2+q^{-2}-2\cos\frac{\pi(k-l)}{L})}\,. \tag{3.1.24}$$

For $q\rightarrow 1$(symmetric diffusion) this expression reduces to Eq. (3.1.21). The other two parts depend on the input rates p_l, p_r and read

$$f^{(L)}_{k,l} \;=\; \frac{\sin\frac{\pi k}{L}\,\sin\frac{\pi l}{L}\,(\cos\frac{\pi l}{L}-\cos\frac{\pi k}{L})}{2\,(q+q^{-1}+p_l-2\cos\frac{\pi k}{L})\,(q+q^{-1}+p_l-2\cos\frac{\pi l}{L})} \tag{3.1.25}$$

$$f^{(R)}_{k,l} \;=\; \frac{(-)^{k+l+1}\,q^{-2L}\,\sin\frac{\pi k}{L}\,\sin\frac{\pi l}{L}\,(\cos\frac{\pi l}{L}-\cos\frac{\pi k}{L})}{2\,(q+q^{-1}+p_r-2\cos\frac{\pi k}{L})\,(q+q^{-1}+p_r-2\cos\frac{\pi l}{L})} \tag{3.1.26}$$

The inhomogeneous solution of the difference equations (3.1.6)-(3.1.9) is then obtained by inserting Eq. (3.1.23) into Eq. (3.1.20).

For a fixed value of the lattice length L the holes probability function depends on three parameters: p_l, p_r and q. By reversing the ends of the lattice one sees that:

$$\Omega(j\,,m\,,p_l\,,p_r\,,q) \;=\; \Omega(L-m+1\,,L-j+1\,,p_r\,,p_l\,,q^{-1}) \tag{3.1.27}$$

Due to (3.1.23) the holes probability function obeys the following rule:

$$\Omega(j\,,m\,,p_l\,,p_r\,,q) \;=\; \Omega(j\,,m\,,p_l\,,0\,,q) \;+\; \Omega(L-m+1\,,L-j+1\,,p_r\,,0\,,q^{-1}) \;-\; \Omega(j\,,m\,,0\,,0\,,q) \tag{3.1.28}$$

Therefore it will be sufficient to study systems with particle input at only one boundary. Using (3.1.28) one can relate physical quantities referring to systems with particle input at both ends with the ones computed for systems for which p_l or p_r is 0. As an example, the particle concentration at site j

$$c(j) \;=\; 1 \;-\; \Omega(j-1\,,j) \tag{3.1.29}$$

can be written as a sum (3.1.28):

$$c(j\,,p_l\,,p_r\,,q) \;=\; c(j\,,p_l\,,0\,,q) \;+\; c(L-j+1\,,p_r\,,0\,,q^{-1}) \;-\; c(j\,,0\,,0\,,q) \tag{3.1.30}$$

Here $c(j,0,0,q)$ is the particle concentration in the stationary state for input rates 0, i.e. it is the particle concentration of one random walker occupying the whole lattice (3.1.74).

3.1.2 The thermodynamic limit

The formulas derived in the last Section are exact solutions for finite chains. We consider the thermodynamical limit. In this limit the right boundary is moved to infinity while the observer stays in a fixed distance j to the left boundary. We consider systems with no particle input at the right end ($p_r = 0$). We are left with only two parameters, namely the input rate at the left boundary $p \equiv p_l$ and the asymmetry parameter q. Carrying out the limit $L \to \infty$ in Eqs. (3.1.23)-(3.1.26) one is led to a simple integral representation of the one-hole probabilities $\Omega(j,m)$. To this end it is convenient to introduce the quantities μ_z

$$\mu_z \;=\; \frac{1}{2}(q+q^{-1}-iz) - \sqrt{\frac{1}{4}(q+q^{-1}-iz)^2-1} \tag{3.1.31}$$

and its inverse

$$\mu_z^{-1} \;=\; \frac{1}{2}(q+q^{-1}-iz) + \sqrt{\frac{1}{4}(q+q^{-1}-iz)^2-1}\,. \tag{3.1.32}$$

Using this notation, the one-hole probabilities in the thermodynamic limit are given by the elliptic integral

$$\Omega(j,m) \;=\; 1 - \frac{q^{j+m}}{2\pi i}\int_{-\infty}^{+\infty} dz\,\Big(\frac{1}{z}-\frac{z}{z^2+p^2}\Big)\Big(\mu_z^j\mu_{-z}^m - \mu_z^m\mu_{-z}^j\Big)\,. \tag{3.1.33}$$

A proof of this formula is given in Appendix A where also the particle concentration at the first few sites for infinite input rate is computed exactly. Let us now investigate the asymptotic behavior of the particle concentration

$$c(j) \;=\; \frac{1}{2\pi i\,q}\int_{-\infty}^{+\infty} dz\,\Big(q^2\mu_z\mu_{-z}\Big)^j\Big(\frac{1}{z}-\frac{z}{z^2+p^2}\Big)\Big(\mu_z^{-1}-\mu_{-z}^{-1}\Big) \tag{3.1.34}$$

for large j. Three cases have to be considered separately:

i) Symmetric case ($q=1$):
For $q=1$ the logarithm of the expression $\mu_z\mu_{-z}$ in Eq. (3.1.34) can be expanded to first order in z by

$$\log(\mu_z\mu_{-z}) \;=\; -\sqrt{2|z|} + O(|z|^{3/2}) \tag{3.1.35}$$

Rewriting the integral (3.1.34) by

$$c(j) \;=\; \frac{1}{2\pi i}\int_{-\infty}^{+\infty} dz\,\exp\Big(-\sqrt{2|z|}\;j\Big)\,r(j,z) \tag{3.1.36}$$

$$r(j,z) \;=\; \exp(\sqrt{2|z|}\;j)\,(\mu_z\mu_{-z})^j\Big(\frac{1}{z}-\frac{z}{z^2+p^2}\Big)\Big(\mu_z^{-1}-\mu_{-z}^{-1}\Big) \tag{3.1.37}$$

and expanding $r(j,z)$ in z the integral can be solved order by order. We obtain the series

$$c(j) \;=\; \frac{2}{\pi j}+\frac{1}{\pi j^2}-\frac{1}{2\pi j^4}+\left(\frac{3}{8\pi}-\frac{12}{\pi p^2}\right)\frac{1}{j^5}+O(j^{-6}) \tag{3.1.38}$$

This proves that in the fermionic case the first three terms in the large x expansion are independent of the input rate p.

ii) Bias to the right ($q>1$):
In this case we find that the expression $\log(q^2\mu_z\mu_{-z})$ in Eq. (3.1.34) can be expanded in first order by:

$$\log(q^2\mu_z\mu_{-z}) \;=\; -q^2\frac{q^2+1}{(q^2-1)^3}\,z^2-O(z^4)\,. \tag{3.1.39}$$

Rewriting the integral (3.1.34) by

$$c(j) \;=\; \frac{1}{2\pi i\, q}\int_{-\infty}^{+\infty} dz\,\exp\Big(-q^2\frac{q^2+1}{(q^2-1)^3}\,j\,z^2\Big)\,s(j,z) \tag{3.1.40}$$

$$s(j,z) \;=\; \exp\Big(q^2\frac{q^2+1}{(q^2-1)^3}\,j\,z^2\Big)\Big(\frac{1}{z}-\frac{z}{z^2+p^2}\Big)(q^2\mu_z\mu_{-z})^j\left(\mu_z^{-1}-\mu_{-z}^{-1}\right) \tag{3.1.41}$$

and expanding $s(j,z)$ in z the integral can be solved again order by order. We obtain

$$c(j) \;=\; \sqrt{\frac{q^2-1}{(q^2+1)\pi j}}\left[1+\left(\frac{3q^4+20q^2-1}{8(q^4-1)}-\frac{(q^2-1)^3}{2q^2(q^2+1)p^2}\right)\frac{1}{j}\right]+O(j^{-5/2}) \tag{3.1.42}$$

We notice that, as opposed to the symmetric case, only the leading term is independent of the input rate.

iii) Bias to the left $q<1$:
If the particles hop preferentially to the left, they accumulate at the left boundary and thus we expect an exponential decay of the concentration profile. In fact, as can be seen from Eq. (3.1.34), the expression $q^{2j-1}c(j)$ is invariant under the replacement $q\to q^{-1}$. This means that for a bias directed towards the left boundary the concentration profile decays like $q^{4j}j^{-1/2}$:

$$c(j) \;=\; q^{4j}\left(\sqrt{\frac{1-q^2}{(q^2+1)\pi j}}+O(j^{-3/2})\right) \tag{3.1.43}$$

We would like to remark that the series presented in this Section are *asymptotic series* since they are derived from an elliptic integral.

3.1.3 The continuum limit

An alternative way to describe the physics of the coagulation model with an external input source is to consider the continuum limit of the one-hole equations. This can be done by taking the lattice spacing $\lambda\to 0$ while keeping the two quantities

$$\hat{r}=\frac{2\,(q-q^{-1})}{\lambda\,(q+q^{-1})} \qquad \text{and} \qquad \hat{p}=\frac{2p_l}{\lambda^2(q+q^{-1})} \tag{3.1.44}$$

constant. We then replace the empty-hole probabilities $\Omega(x,y)$ by their continuous counterparts:

$$\Omega^c(x,y) \;=\; \Omega(\frac{j}{\lambda},\frac{m}{\lambda}) \tag{3.1.45}$$

It is useful to rescale the hole density function taking $\hat{\Omega}(x,y) = \Omega^c(x,y)e^{-\frac{\hat{r}}{2}(x+y)}$ which verifies the equation (see Eq.(3.1.6))

$$\Big(\Delta - \frac{\hat{r}^2}{2}\Big)\,\hat{\Omega}(x,y) \;=\; 0 \qquad\qquad (L > y > x > 0) \tag{3.1.46}$$

By solving the continuous counterparts of Equations (3.1.2)-(3.1.4) we determined the value of the holes density function on the boundaries. The solutions are:

- Along the left boundary ($x = 0\ ,\ 0 \le y \le L$):

$$\hat{\Omega}(0,y) \;=\; \begin{cases} \dfrac{\sinh\Big((L-y)\sqrt{\frac{\hat{r}^2}{4}+\hat{p}}\Big)}{\sinh\Big(L\sqrt{\frac{\hat{r}^2}{4}+\hat{p}}\Big)} & \text{if } \hat{p} \neq \infty \\ 0 & \text{if } \hat{p} = \infty \end{cases} \tag{3.1.47}$$

- Along the upper boundary ($y = L\ ,\ 0 \le x \le L$):

$$\hat{\Omega}(x,L) \;=\; \begin{cases} \dfrac{e^{-\hat{r}L}\sinh\big(\frac{\hat{r}}{2}x\big)}{\big(\sinh\frac{\hat{r}}{2}L\big)} & \text{if } \hat{r} \neq 0 \\ x/L & \text{if } \hat{r} = 0 \end{cases} \tag{3.1.48}$$

- On the diagonal ($0 \le x = y, \le L$) the normalisation condition is:

$$\hat{\Omega}(x,x) \;=\; e^{-\hat{r}x}\,. \tag{3.1.49}$$

Equation (3.1.46) together with the boundary conditions (3.1.47)-(3.1.49) define a Dirichlet problem for the function $\hat{\Omega}(x,y)$. The formal solution is

$$\hat{\Omega}(x,y) \;=\; \oint_C ds\,\hat{\Omega}(x',y')\frac{\partial}{\partial n}\,\mathcal{G}(x,y,x',y') \tag{3.1.50}$$

where C is the contour along the boundaries, $\frac{\partial}{\partial n}$ the normal derivative and $\mathcal{G}(x,y,x',y')$ the Green function defined by

$$\Big(\Delta - \frac{\hat{r}^2}{2}\Big)\mathcal{G}(x,y,x',y') = \delta(x-x')\delta(y-y') \tag{3.1.51}$$

$$\mathcal{G}(0,y,x',y') = \mathcal{G}(x,y,0,y') = \mathcal{G}(x,L,x',y') = \mathcal{G}(x,y,x',L) = 0 \tag{3.1.52}$$

$$\mathcal{G}(x,x,x',y') = \mathcal{G}(x,y,x',x') = 0 \tag{3.1.53}$$

The computation of the density function of the hole probabilities requires the computation of the Green function. This was done in two steps. First notice that:

$$\mathcal{G}(x,y,x',y') = \mathcal{G}_\square(x,y,x',y') - \mathcal{G}_\square(y,x,x',y') \tag{3.1.54}$$

where $\mathcal{G}_\Box(x,y,x',y')$ is the Green function of the Dirichlet problem defined in the interior of the square $0 \le x \le L$, $0 \le y \le L$. $G_\Box$ can be constructed easily by using reflection techniques. All what one needs to know is the Green function of the Dirichlet problem defined on the entire plane (with boundaries at infinity). We denote the last mentioned function with $g(x,y,x',y')$. Summing up, we get:

$$\mathcal{G}(x,y,x',y') = \sum_{\alpha,\beta=\pm 1} \alpha\beta \sum_{i,j=-\infty}^{+\infty} \Big[g\left(\sqrt{(x-2iL-\alpha x')^2 + (y-2jL-\beta y')^2}\right) - g\left(\sqrt{(y-2iL-\alpha x')^2 + (x-2jL-\beta y')^2}\right) \Big] \tag{3.1.55}$$

Once the density function $\hat{\Omega}(x,y)$ is known one can compute expectation values of observables in the steady state. The local particle density is given by

$$\rho(x) = \lim_{y\to x} \frac{1 - e^{\frac{\hat{r}}{2}(x+y)}\,\hat{\Omega}(x,y)}{y-x} = -\frac{\partial}{\partial y}\,\Omega^c(x,y)\Big|_{y=x} . \tag{3.1.56}$$

We also give a closed formula for the computation of the connected two-point function:

$$G^c(x,y) = \langle n_x n_y \rangle - \langle n_x \rangle \langle n_y \rangle \tag{3.1.57}$$

Here n_x denotes the particle number operator at site x. Using the factorization properties of the two-holes probability function mentioned in [30, 31] it is easy to see that in the continuum limit we have:

$$G^c(x,y) = \frac{\partial}{\partial x}\Omega^c(x,y)\frac{\partial}{\partial y}\Omega^c(x,y) - \Omega^c(x,y)\frac{\partial^2 \Omega^c(x,y)}{\partial x \partial y} \tag{3.1.58}$$

The scaling limit in the symmetric case ($q = 1$)

In the case of symmetric diffusion the differential equation (3.1.46) reduces to a Laplace equation. The Green function can be obtained from (3.1.55) by replacing $g(u)$ with $\frac{1}{2\pi}\ln u$.

Let us consider for simplicity first the case of an *infinite particle input* rate ($\hat{p} = \infty$). In this case the hole density function is zero for $x = 0$ (see Eq. (3.1.47)). We are left with:

$$\Omega^c_\infty(x,y) = \int_0^L du \left(\frac{\partial}{\partial x'} - \frac{\partial}{\partial y'}\right) \mathcal{G}(x,y,x',y')\Big|_{x'=y'=u} - \int_0^L dx' \,\frac{x'}{L}\frac{\partial}{\partial x'}\mathcal{G}(x,y,x',y')\Big|_{y'=L} \tag{3.1.59}$$

Inserting Eq. (3.1.55) one is led to

$$\Omega^c_\infty(x,y) = \sum_{\alpha,\beta=\pm 1}\alpha\beta \sum_{i,j=-\infty}^{+\infty} \Big[\arctan\Big(\frac{\alpha(2i - x/L) - \beta(2j - y/L)}{(2i - x/L)^2 + (2j - y/L)^2 + \alpha(2i - x/L) + \beta(2j - y/L)}\Big) - \Big(\beta(i - \frac{x}{2L}) + \alpha(j - \frac{y}{2L})\Big)\arctan\frac{\alpha + 2i - x/L}{\beta + 2j - y/L}\Big] . \tag{3.1.60}$$

We see that the hole density function for $\hat{p} = \infty$ depends only on x/L and y/L . From Eq. (3.1.56) we obtain the local particle density in the stationary state for *infinite* particle input rate:

$$\rho_\infty(x) = \frac{2}{\pi L}\sum_{i,j=-\infty}^{+\infty} \frac{(x/L - 2i) + (x/L - 2j)}{(x/L - 2i)^2 + (x/L - 2j)^2} \tag{3.1.61}$$

Defining $z = \frac{x}{L}$, Eq.(3.1.61) can be rewritten as

$$L\rho_\infty(x) \;=\; \Phi(z) \tag{3.1.62}$$

where

$$\begin{aligned}
\Phi(z) \;&=\; \frac{1}{\pi}\sum_{i,j=-\infty}^{+\infty} \frac{(z/2-i)+(z/2-j)}{(z/2-i)^2+(z/2-j)^2} \;= \qquad\qquad (3.1.63)\\
&=\; \frac{\sinh(\pi z)\,+\,\sin(\pi z)}{\cosh(\pi z)\,-\,\cos(\pi z)} \;+\; \sum_{k=1}^{+\infty}\left\{\frac{\sinh(2\pi(z/2-k))\,+\,\sin(\pi z)}{\cosh(2\pi(z/2-k))\,-\,\cos(\pi z)} \;+\;(\,k\;\longleftrightarrow\;-k\,)\right\}.
\end{aligned}$$

The function $\Phi(z)$, called scaling function, is odd and periodic with period 2. In the limit $z \to 0$ the function diverges like $\frac{2}{\pi z}$ (the dominant contribution is given by the first term in the second line of (3.1.63)). For $z \to 1$, $\Phi(z)$ approaches the value 1, but the value itself in the point $z = 1$ is $\Phi(1) = 0$. So the function is discontinuous for all integer arguments.

We consider now the case of an arbitrary input rate $\hat{p}$ and look at the scaling regime (z fixed, $L \to \infty$). If $\hat{p}$ is finite one picks up another contribution to the holes density function coming from the integration along the boundary segment ($x = 0$, $0 \leq y \leq L$) in (3.1.50). The difference between the values of the holes density function corresponding to infinite and finite input rates is:

$$\Omega^c_\infty(x,y) - \Omega^c_{\hat{p}}(x,y) \;=\; \int_0^L dy'\;\Omega^c_{\hat{p}}(0,y')\,\frac{\partial}{\partial x'}\mathcal{G}(x,y,x',y')\bigg|_{x'=0} \tag{3.1.64}$$

We are here interested in the scaling and thermodynamical limit. For large values of the lattice length L , $\Omega^c_{\hat{p}}(0,y')$ behaves like $\exp(-y'\sqrt{\hat{p}})$. We expand the derivative of the Green function in Eq. (3.1.64) near $y' = 0$ and get:

$$\begin{aligned}
\Omega^c_\infty(x,y) - \Omega^c_{\hat{p}}(x,y) \;&=\; \frac{16}{\pi}\sum_{i,j=-\infty}^{+\infty} \frac{(x/L-2i)(y/L-2j)\Big[(y/L-2j)^2\,-\,(x/L-2i)^2\Big]}{\Big[(y/L-2j)^2\,+\,(x/L-2i)^2\Big]^4}\times\\
&\int_0^1 \frac{\sinh\left(\sqrt{\hat{p}}L(1-u)\right)}{\sinh\left(\sqrt{\hat{p}}\;L\right)}\Big(\,u^3\,+\,O(u^7)\,\Big)du
\end{aligned}$$

It is easy to see that in the finite-size scaling limit one gets:

$$\Phi_{\hat{p}}(z) \;=\; \Phi(z) \,+\, \frac{1}{L^4}\Phi^{\rm corr}(z) + O\Big(\frac{1}{L^8}\Big)\,. \tag{3.1.65}$$

The first finite-size scaling correction function is

$$\Phi^{\rm corr}(z) \;=\; \frac{3}{\pi\hat{p}^2}\sum_{i,j=-\infty}^{+\infty}(z/2-i)\frac{(z/2-i)^4-10(z/2-i)^2(z/2-j)^2+5(z/2-j)^4}{\Big[(z/2-i)^2+(z/2-j)^2\Big]^5} \tag{3.1.66}$$

So we proved that in the scaling limit the particle density function scales. The scaling function $\Phi(z)$ given by equation (3.1.63) is independent on the input rate. We get finite-size corrections of order L^{-4} for finite input rates.

In Figure 3.2 we show the function (solid curve)

$$F(z) \;=\; \frac{\pi z}{2}\cdot\Phi(z) \tag{3.1.67}$$

(with this definition $F(0) = 1$) together with finite-lattice calculations (see Eqs. (3.1.29) and (3.1.20)) obtained for $L = 2000$ ($p = 1$) and for $L = 800$ ($p = \infty$). We have given this figure for two reasons. First we observe that the scaling function has a nontrivial behavior at the opened end of the system ($z \propto 1$). Next, although the scaling function was computed in the continuum limit, it applies to the lattice too.

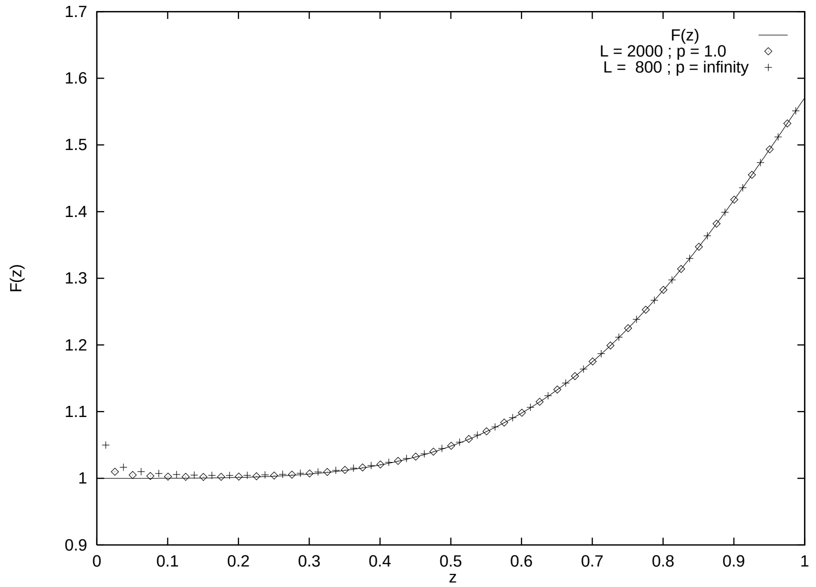

Figure 3.2: The function $F(z)$ defined by Eq. (3.1.67) (solid curve) compared to lattice calculations for $L = 2000$ ($p = 1.0$) and $L = 800$ ($p = \infty$).

Let us consider the *thermodynamical limit* $L \to \infty$, x fixed. Using equations (3.1.56) and (3.1.55) (from the multiple sum of the latter one we take only the terms corresponding to $i = j = 0$) one can show that

$$\rho(x) \; = \; \frac{2}{\pi x} - \frac{12}{\pi \hat{p}^2 x^5} + \frac{5040}{\pi \hat{p}^4 x^9} + O(p^{-6} x^{-13})\,. \tag{3.1.68}$$

The asymptotic behavior (for large values of x) of the one-point function in the thermodynamical limit (3.1.68) can be also obtained from the scaling behavior (3.1.65), in the limit $z \to 0$. The result (3.1.68) is consistent with the expansion for the stationary concentration profile on a discrete lattice (3.1.38). The only difference is that in the continuum limit all contributions $\frac{1}{x^i p^j}$ with $i > 2j + 1$ scale like λ^{i-2j-1} and therefore vanish in the limit of vanishing lattice spacing $\lambda \to 0$.

We mention one last result concerning the connected two-point function. In the thermodynamical limit one can see (c.f. Ref. [31]) that the hole probability density for infinite input rate is:

$$\Omega^c_\infty(x, y) \; = \; \frac{4}{\pi} \arctan\Big(\frac{x}{y}\Big) \tag{3.1.69}$$

Using (3.1.58) one gets the following expression for the connected two-point-function

$$G^c(x, x+d) \; = \; -\frac{16}{\pi^2}\frac{1}{x^2}\frac{\left[1+v-v(2+v)\,\arctan\left(\frac{1}{1+v}\right)\right]}{(2+2v+v^2)^2} \tag{3.1.70}$$

in the infinite input rate case. On the right hand side of (3.1.70) we denoted $\frac{d}{x}$ with v. Notice again the algebraic fall-off.

Bias to the right $(\hat{r} > 0)$

Writing the Fourier transform of (3.1.51) one gets

$$g(u) \; = \; -\frac{1}{(2\pi)^2}\int_0^\infty \frac{k \cdot dk}{k^2+\hat{r}^2/2}\int_0^{2\pi} e^{-iku\cos\theta} d\theta\,. \tag{3.1.71}$$

Thus the Green function of the problem defined on the entire plane is (see formulae (9.6.16) in [33] and (6.532.4) in [34])

$$g(u) \; = \; -\frac{1}{2\pi}\,K_0\Big(\sqrt{\frac{\hat{r}^2}{2}}u\Big) \tag{3.1.72}$$

We use the standard notation $K_i\,,\; i = 0, 1, 2...$ for the modified Bessel functions.

In Appendix B we will prove that in the thermodynamical limit the asymptotic behavior of the particle density is given by

$$\rho(x) \; = \; \sqrt{\frac{\hat{r}}{2\pi x}} + \frac{1}{4\sqrt{2\pi\hat{r}}}\left[\frac{11}{2} - \frac{\hat{r}^4}{\hat{p}^2}\right]\frac{1}{x^{3/2}} \; + \; O(x^{-5/2}) \tag{3.1.73}$$

The leading term is the continuum correspondent of the one appearing in Eq. (3.1.42) and is independent of the input rate.

We conclude this Section with some remarks concerning the influence of the right boundary on the particle density.

As opposed to the symmetric case, one can check that for biased diffusion to the right the behavior of the one point function in the thermodynamical limit is identical with the one in the scaling limit. One can give a qualitative explanation. In the stationary state, near the right boundary, the density function can be approximated with the one given by a single particle occupying the whole lattice (a random walker)

$$c(y) \; = \; \begin{cases} q^{-2y}\frac{1-q^{-2}}{1-q^{-2L}} & \text{for } q \neq 1 \\[2ex] \frac{1}{L} & \text{for } q = 1 \end{cases} \tag{3.1.74}$$

where $y = L - x$.

For biased diffusion to the right the density decays exponentially in y. So the influence of the right boundary is of short range and is not seen in the scaling limit.

For $q = 1$ (or $\hat{r} = 0$) the influence of the right boundary is much stronger. The density determined by a random walker near the right end of the lattice is constant $(\frac{1}{L})$ and greater than the one obtained through the extrapolation of Eq. (3.1.38) ($\frac{2}{\pi L}$). This explains the linear behavior of the reduced scaling function for $z \to 1$ (see Figure 3.2).

One can also notice from the y and L dependence of $c(y)$ that one has a characteristic length scale $\Lambda = (2\ln q)^{-1}$ which is related to the inverse mass seen in the spectrum of the Hamiltonian (see Eq. (3.1.18)). This observation is very interesting since it clarifies a puzzle which goes through this chapter: how can a system with massive excitations in the time direction show an algebraic and, as we shall see in the next Section, universal behavior? The answer is that one looks at the concentration in the "wrong" way following the x dependence (away from the source) and not the y dependence (away from the open end). The discovery that this "wrong" way exists is probably the main achievement of the study presented in this chapter.

3.2 Numerical verification of the universality hypothesis

In this Section we present the results of Monte Carlo simulations. The details are given in Appendix C. We restrict the study to cases for which $p_r = 0$ and $r \geq 0$. We start with the case of symmetric diffusion ($q = 1$ or $r = 0$). First we look at the density profile ($1 \ll x \ll L$). As suggested by Eq.(3.1.38), we fit the data by the function

$$c(x) = \frac{K_1}{x} + \frac{K_2}{x^2} + \frac{K_3}{x^3}. \tag{3.2.1}$$

When making the fits (by using the χ^2 method) we took points $x \in [L/10, L/2]$ in order to avoid finite-size effects. The estimates for K_1 and K_2 for various input and bulk rates are given in Table (I). The data presented here were obtained taking lattices of size $L = 1000$.

s	t	p	K_1	K_2
0.50	0	1	0.635 ± 0.001	10.2 ± 0.2
0.50	0	∞	0.639 ± 0.004	9.8 ± 0.8
0.50	-0.2	1	0.640 ± 0.010	16 ± 5
0.50	-0.2	∞	0.640 ± 0.010	13 ± 3
0.25	0	1	0.637 ± 0.002	22 ± 4
0.25	0	∞	0.632 ± 0.002	24.4 ± 0.4
0.40	-0.2	1	0.638 ± 0.002	11 ± 2
0.40	-0.2	∞	0.642 ± 0.004	10.4 ± 0.6

Table I: Estimates of the coefficients K_1 and K_2 of the expression (3.2.1) for various input and bulk rates

We notice that K_1 is everywhere close to the value obtained in the fermionic case ($s = 2,\ t = 0$) namely $K_1 = 2/\pi \simeq 0.637$. The values of K_2 are different if the bulk rates are different but as in the fermionic case they do not depend on the input rate.

Since the leading term of the density profile is compatible with universality, one can go one step further and check if the scaling function $\Phi(z)$ given by Eq. (3.1.63) in the fermionic case, is also universal. This function was obtained taking $x/L = z$ fixed (x and L large):

$$\lim_{L\to\infty} Lc(z, L) = \Phi(z) \tag{3.2.2}$$

We define the function

$$K(z,L) \;=\; \frac{L\,c(z,L)}{\Phi(z)} - 1 \tag{3.2.3}$$

which measures the deviation from universality and the finite-size effects. In Fig. 3.3 we give the data in the case $p=1\,, s=0.5\,, t=0$ for three lattice sizes. One notices that with increasing lattice size $K(z,L)$ decreases, as it should. One should mention that for $z=0$ one expects $K(z,L)$ to go to zero in the limit $L \to \infty$ because of the universality of K_1 in Eq.(3.2.1) and the uniform convergence of $\Phi(z)$ in the fermionic case. Thus the relative large values of $K(z,L)$ observable in Fig. 3.3 for small values of z should not be a subject of concern. We have also done other simulations (not shown in Figure 3.3) for other input rates which show the same properties.

In Figure 3.4, $K(z,L)$ is shown for various input and coagulation rates for a lattice of length $L=1000$. As one can see $K(z,L)$ is small everywhere (for small values of z the convergence is slow but as mentioned above, for $z=0$ universality was checked already).

We now consider the asymmetric diffusion case ($q>1$). As suggested by Eq. (3.1.42) we fit the Monte Carlo data by the function

$$c(x) \;=\; K'_{1/2}x^{-1/2} \,+\, K'_1 x^{-1} \,+\, K'_{3/2}x^{-3/2}\,. \tag{3.2.4}$$

We choose $q=\sqrt{2.5}$ (which corresponds to $r=0.857$), in which case we get from Eq. (3.1.42) $K'_{1/2}=\sqrt{\frac{3}{7\pi}} \simeq 0.369$. Notice that we have allowed a term $\sim x^{-1}$ not present in Eq. (3.1.42). The data were collected for $L=1000$ and the results are shown in table II.

s	t	p	$K'_{1/2}$	K'_1
1.000	0.429	1	0.370 ± 0.003	0.10 ± 0.01
1.000	0.429	∞	0.368 ± 0.002	0.11 ± 0.01
0.500	0.214	1	0.368 ± 0.003	0.90 ± 0.04
0.500	0.214	∞	0.369 ± 0.004	0.82 ± 0.07
0.250	0.107	1	0.369 ± 0.002	2.12 ± 0.02
0.250	0.107	∞	0.369 ± 0.002	2.09 ± 0.02
0.361	-0.181	1	0.368 ± 0.001	1.27 ± 0.02
0.361	-0.181	∞	0.369 ± 0.003	1.25 ± 0.04

Table II: The coefficient $K'_{1/2}$ and K'_1 of the expansion (3.2.4) for various input and coagulation rates. All data are for $q=\sqrt{2.5}$ ($r=0.857$).

As can be seen from this table the coefficient $K'_{1/2}$ is unchanged (universal). The K'_1 is independent on the input, but depends on the bulk rates (similar to the K_2 coefficient in Eq. (3.2.1)). Finally we notice that the values of K'_1 get smaller if we approach the fermionic case ($r=t=0.857,\ s=2$).

To sum up, in the symmetric diffusion case the Monte Carlo data suggest that the large x behavior and the scaling function are universal: they are independent of the Γ^{11}_{10}, Γ^{11}_{01} and p rates. In the asymmetric diffusion case, the large x behavior is also universal.

In the following pages two figures are displayed:

- Figure 3.3 The L dependence of the $K(z,L)$ function define by Eq. (3.2.3) for $p = 1.0$, $s = 0.5$, $r = t = 0$. If the scaling function is universal, $K(z,L)$ should vanish in the thermodynamical limit. (Monte Carlo simulations)
- Figure 3.4 The $K(z,L)$ function for $L = 1000$, $r = 0$ and different input and coagulation rates. (Monte Carlo simulations)

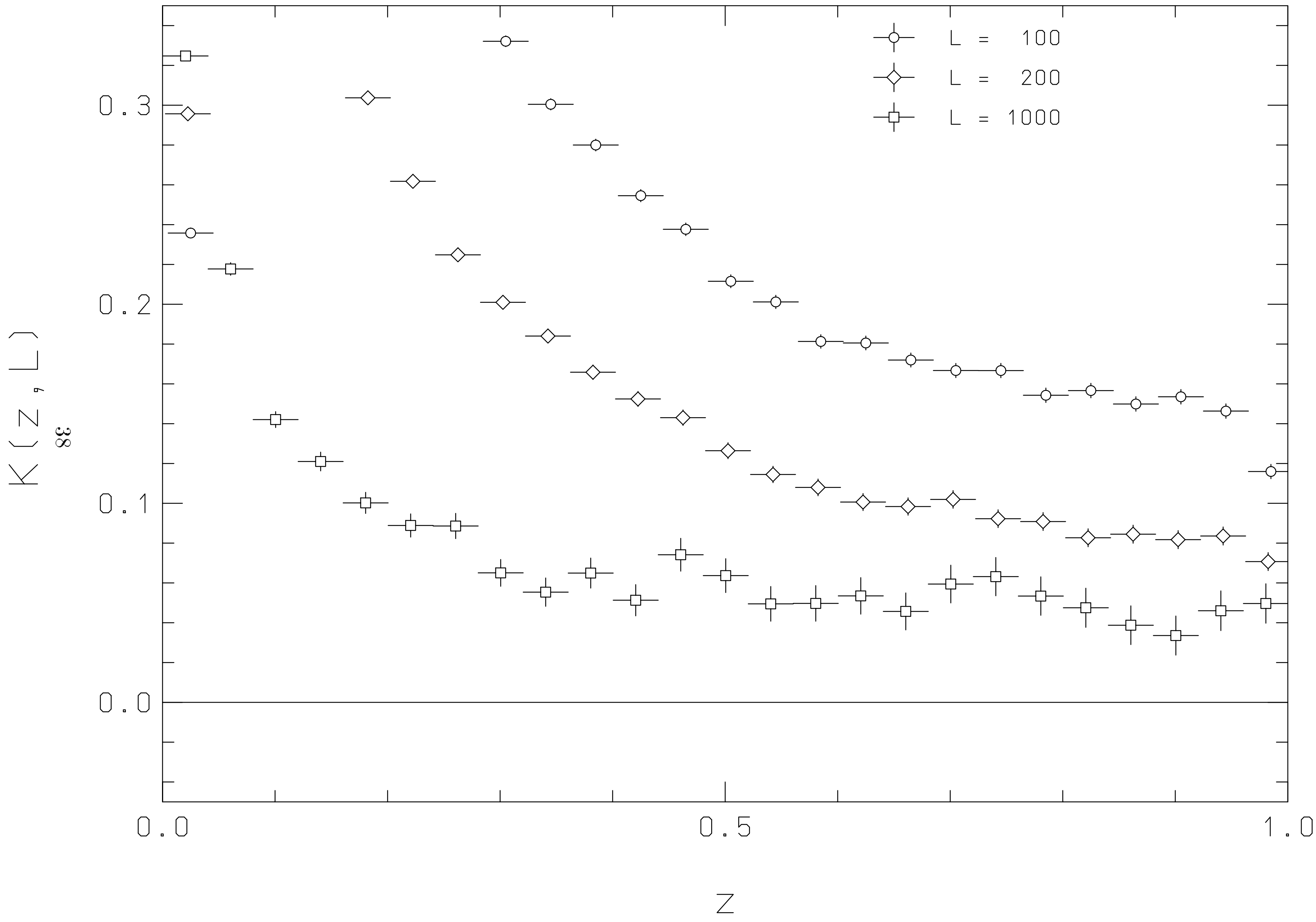
L = 100
L = 200
L = 1000
0.0
0.1
0.2
0.3
K(z,L)
0.0
0.5
1.0
z

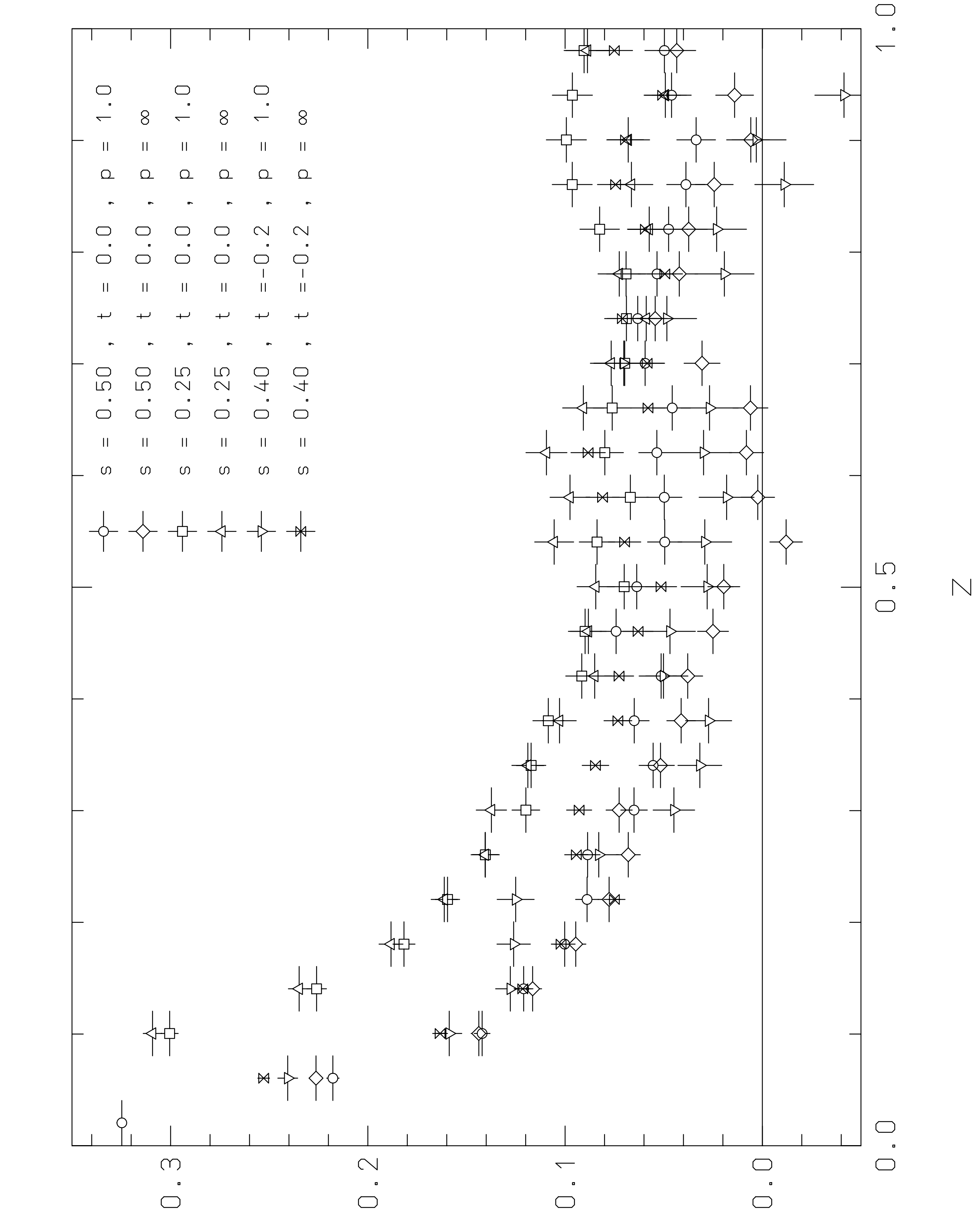
s = 0.50 , t = 0.0 , p = 1.0
s = 0.50 , t = 0.0 , p = ∞
s = 0.25 , t = 0.0 , p = 1.0
s = 0.25 , t = 0.0 , p = ∞
s = 0.40 , t =-0.2 , p = 1.0
s = 0.40 , t =-0.2 , p = ∞
0.0
0.1
0.2
0.3
0.5
1.0
K(Z,L)
Z

Chapter 4

Similarity Transformations and the Dynamic of Annihilation-Coagulation Systems

One-dimensional reaction-diffusion models [1] have been used in explaining certain features of some experimental results [35, 36, 6, 37]. In these experiments the exciton propagation is studied. The conclusion drawn from the measurements is that this propagation takes place in one dimension along structures like molecular "wires" and chains. The luminescence decay at early times is algebraic:

$$c(t) \propto \frac{1}{t^{\alpha}} \quad \text{with } \alpha = 1/2. \tag{4.0.1}$$

This observation yields the conjecture that exciton-exciton annihilation processes take place [37]. However, it is not clear whether exciton-exciton coagulation (fusion) reactions happen. In both the annihilation and coagulation chemical models the long-time behavior of the concentration obeys (4.0.1). Moreover, we will prove that this asymptotic behavior of the concentration is common to all models in which both reactions take place (4.2.10). We call them annihilation-coagulation systems. The coefficient of the leading term depends on the on the ratio of the rates of these two processes. In this chapter we consider left-right symmetric models (i.e. systems for which $\Gamma^{\alpha,\beta}_{\gamma,\delta} = \Gamma^{\beta,\alpha}_{\delta,\gamma}$) if not else specified. We show that all exciton reaction rates can be determined from experimental data. In our study we use a numerical and an analytical approach:

First we want to determine the next to leading term in the long-time expansion of the concentration in the coagulation model. Three results are given in the literature concerning this regime. An approximative equation for the particle concentration derived from empty interval probabilities is obtained in [38]. A approximation scheme applied to an diffusion-type equations is used in [39]. These two approaches lead to almost the same conjecture:

$$c(t) = \sqrt{\frac{1}{2\pi t}} + \frac{R}{\pi t}\frac{\Delta'}{1-\Delta'} + O(t^{-x}) \tag{4.0.2}$$

where $R = 1$ in [39] and $R = \pi/4 \simeq 0.786$ in [38]. Here $1 - \Delta'$ is the coagulation rate. The time scale in which the diffusion rate is equal to one is chosen. The coefficient of the leading term was

[1] This Chapter is entirely based on Ref. [27].

exactly computed for $\Delta' = \emptyset$ [3]. In this case the next to leading term is of order $t^{-3/2}$ [13] and the operator which appears in the master equation is the Hamiltonian of a supersymmetric system [2].

We verify the conjecture (4.0.2) by determining the value of the coefficient of the next to leading term in the $\Delta' \neq \emptyset$ case. It can be computed by solving the Bethe Ansatz equations for the XXZ chain in an external field [2]. However this computation is a mathematical challenge because one needs to know both the spectra and the eigenvectors of the Hamiltonian. Here we investigate this problem with the help of Monte Carlo simulations. The numerical data presented in Section 4.3 strongly support the $R = 1$ conjecture.

Secondly, we want to find all chemical models which can be described with the help of (4.0.2) and other results concerning the coagulation model. We do this by looking for similarity transformations which map the coagulation model onto other reaction-diffusion systems. In [3, 4, 5] it was shown that the one-species annihilation and coagulation systems belong to the same universality class. A general proof is given within the framework of the "Hamiltonian" formalism. The operators which appear in the master equations describing the two models are the Hamiltonians of quantum chains [2] and are equivalent. We say that two reaction-diffusion systems are equivalent when the corresponding Hamiltonians can be obtained one from the other through a similarity transformation [13]. In this chapter we apply this method and look for further transformation which connect chemical models and lead to linear relations among their observables. Thus one can extend results concerning one reaction-diffusion systems to all its equivalent ones. In other words: we start from one system and look for other systems belonging to the same universality class.

We prove that the one-species coagulation-annihilation models can be divided in equivalence classes with respect to one parameter. Each class contains also a pure coagulation and a pure annihilation model.

Another reaction-diffusion system which has attracted much attention is the two species annihilation model ($A + B \longrightarrow \emptyset + \emptyset$). Scaling considerations indicate that, for equal initial site occupation probabilities of the two species, the concentration decay is algebraic with a time exponent equal to 1/4 [40]. This has been proven in [41]. In [42] it was conjectured that the asymptotic behavior of the concentration depends on its initial value:

$$c_A(t) = c_B(t) = \frac{K' \sqrt{c(0)}}{t^{1/4}} + O(t^{-x}) \quad \text{if } c_A(0) = c_B(0) = c(0), \tag{4.0.3}$$

where $K' = (2\pi)^{-3/4} \simeq 0.252$. A similar result was obtained in [43] through a renormalization group analysis for spatial dimensions higher than two. In this work the conjectured dependence is validated for small values of $c(0)$. A general closure scheme for truncating the hierarchies of the joint density function equations leads to the same formula but with $K' = (32\pi)^{-1/4} \simeq 0.316$ [44]. A value of $K' = 0.28$ has been numerically determined [42]. We report results of Monte Carlo simulations started at low values of the initial concentration. A better estimate for the constant K' is obtained. It is in good agreement with the values conjectured in [42, 43].

We also look for the chemical models equivalent to the two species annihilation reaction-diffusion system.

The chapter is structured as follows:

In section 4.1 a general condition satisfied by the transformations which map reaction-diffusion system among themselves is derived.

In section 4.2 we look for chemical models equivalent to systems previously studied. We concentrate on systems for which the particle concentration was computed.

Two models which the procedure is applied to were mentioned before: the one species coagulation and the two species annihilation reaction-diffusion systems. Another model which is exactly solved in some special case is the coagulation-decoagulation one [10, 13]. We find two reaction-diffusion systems which are equivalent to it: the annihilation-creation and the death-decoagulation models. Thus we can give exact solutions for the particle number in a system in which decoagulation and death processes are permitted, but particles do not diffuse.

In the last section another set of results obtained from Monte Carlo simulations are presented.

4.1 The similarity transformation

The advantage of the Hamiltonian formalism is that we can introduce similarity transformations. Our interest is to find those matrices B for which the transformed Hamiltonian

$$\hat{H} \; = \; \sum_{i=1}^{L} \hat{H}_i \; = \; B\,H\,B^{-1} \tag{4.1.1}$$

describes also the dynamic of a reaction-diffusion system. (The quantities in the transformed model are denoted with a $\hat{}$.) Therefore we have to concentrate on local transformations:

$$B = b \otimes b \otimes \cdots \otimes b \tag{4.1.2}$$

defined by the L-fold tensor product of a real $N \times N$ matrix b. The mapping can easily be extended to the computation of expectation values. They can be computed [13] from the corresponding expectation values in the 'original' model:

$$< \widehat{X} >(|P_0\rangle, t) = \langle 0|X \exp(-\hat{H}t)|P_0\rangle =$$

$$\langle 0|X\,B \exp(-Ht)B^{-1}|P_0\rangle =< X\,B > (B^{-1}|P_0\rangle, t) \tag{4.1.3}$$

Some restrictions have to be imposed on b. First, the sum of the entries from each column of $\hat{H}_i$ must be 0:

$$\langle 0|BH_i = 0 \; . \tag{4.1.4}$$

A general solution of (4.1.4) is:

$$\langle 0|B = \rho\langle 0| \tag{4.1.5}$$

Here ρ is real. We have checked explicitly for every model considered in this chapter that transformations obeying (4.1.4) but not (4.1.5) do not lead to new mappings. Using (1.1.10) and (4.1.2) one gets the restriction:

$$\sum_{i=0}^{N-1} b_{ij} = \rho^{\frac{1}{L}} \; . \tag{4.1.6}$$

We can eliminate a overall scaling parameter by choosing $\rho = 1$. Thus the transformations are represented by real $N \times N$ matrices with the property that the sum of the entries on each column is equal to 1.

Not all these $N \times (N-1)$ - parameter transformations lead to another reaction-diffusion system. The matrix elements of the two sites ($L = 2$) Hamiltonian $\hat{H}$ have to satisfy the following sign conditions:

$$\begin{aligned} \hat{H}_{mm} &\geq 0 \quad m = 0,1\ldots N^2-1 \\ \hat{H}_{mn} &\leq 0 \quad m,n = 0,1\ldots N^2-1,\ m \neq n \end{aligned} \tag{4.1.7}$$

The remaining transformations map reaction-diffusion system one onto the other. The program *REDUCE* was used to compute the transformed Hamiltonians.

4.2 Mappings between reaction-diffusion systems

We will start with the Hamiltonians of those chemical models for which the behavior of the particle concentration is known and look for local transformations which map them onto other reaction-diffusion systems.

There are always the $N!-1$ permutation transformations which interchange (if $N = 3$ different types of) particles and vacancies. We will treat everything "modulo" these permutations.

As we mentioned before, we restrict ourselves to the left-right symmetric case, unless otherwise specified. The similarity transformation preserves this property. The generalization to the non-symmetric case is straightforward.

In the three state model we take equal diffusion rates for the two kinds of particles ($\Gamma^{01}_{10} = \Gamma^{02}_{20}$). One parameter of the problem can be eliminated by choosing the time scale in which the diffusion rates are equal to 1.

4.2.1 Two-state models

Exact results are available for the one-species annihilation, coagulation and coagulation-decoagulation models. For the last two models the system of linear differential equations for the empty interval probabilities was written and solved. These equations decouple from those corresponding to many intervals probabilities [15, 11]. In the transformed models identical systems of equations can be written but for other observables, namely the probabilities of having interpolating sequences of vacancies and particles on consecutive sites [15].

The general form of the local transformation is given by (4.1.6):

$$b = \begin{pmatrix} 1-\alpha & \beta \\ \alpha & 1-\beta \end{pmatrix} \tag{4.2.1}$$

We will start with the annihilation model and not with the equivalent coagulation one. For simplicity we will use the notation a , instead of Γ^{11}_{00}, for the annihilation rate and f for the coagulation rate (Γ^{11}_{10}).

The annihilation model. In this case particles diffuse and disappear pairwise when two of them try to occupy the same site. We denote the corresponding Hamiltonian with $H_{\text{ann.}}$ and introduce, as in [2, 13, 45], the parameter Δ' defined by:

$$\Delta' = 1 - \frac{a}{2}\,. \tag{4.2.2}$$

If $a < 2$, Δ' is equal to the probability that no reaction takes place at an two particles encounter. If the parameter Δ' is zero exact solutions can be obtained because $H_{\mathrm{ann.}}$ can be expressed in terms of free fermions. In [7] the time dependence of the particle concentration is derived in the thermodynamical limit with a full lattice as initial configuration. The finite chain is treated exactly in [2] and the two point correlation functions for the infinite chain are obtained. The particle concentration for random homogeneous initial conditions is deduced in [13].

It can easily be seen that the transformed Hamiltonian $\hat{H}$ will only fulfill the conditions (4.1.7) if at least one of the entries of b is zero. We take $\alpha = 0$. The case $\beta = 0$ can be obtained by applying a permutation transformation on $\hat{H}$.

It is a well known fact [3, 4, 5] that the annihilation and coagulation models are equivalent. We reobtain this result by choosing $\beta = -1$. In this case $\hat{H}$ is identical with the Hamiltonian of the coagulation model [13].

This is, however, only one of the possible choices for the transformation parameter. For $-1 \leq \beta \leq 0$ we get the Hamiltonian of a system in which apart from diffusion with the same rate $\hat{\Gamma}^{10}_{01} = 1$, the following processes are permitted:

- annihilation with rate
$$\hat{\Gamma}^{11}_{00} = \hat{a} = 2\frac{\beta+1}{1-\beta}(1-\Delta')$$
- coagulation with rate
$$\hat{\Gamma}^{11}_{01} = \hat{f} = 2\frac{\beta}{\beta-1}(1-\Delta')$$

The matrix b and Δ' can be written as functions of $\hat{a}$ and $\hat{f}$:

$$\Delta' = 1 - \hat{f} - \hat{a}/2 \tag{4.2.3}$$

or equivalently $a = \hat{a} + 2\hat{f}$. One gets the following result:

$$\hat{H}(\hat{a}, \hat{f}) = B H_{\mathrm{ann.}} B^{-1}$$

where

$$b = \begin{pmatrix} 1 & \frac{-\hat{f}}{\hat{a}+\hat{f}} \\ 0 & \frac{\hat{a}+2\hat{f}}{\hat{a}+\hat{f}} \end{pmatrix} \tag{4.2.4}$$

and with the parameter Δ' (4.2.3).

We have obtained a one-parameter group of similarity transformations which act between annihilation-coagulation models $((a, f) \longrightarrow (\hat{a}, \hat{f}))$ corresponding to the same value of Δ' (i.e. $a/2 + f = \hat{a}/2 + \hat{f}$). It is straightforward to write the transformation which connects the coagulation model ($a = \emptyset$) and one described by $\hat{H}(\hat{a}, \hat{f})$.

Some explicit results concerning the particle concentration can be given now by applying transformations (4.1.3) on formulas obtained for the annihilation ($f = 0$) (4.2.4) or coagulation ($a = 0$) models.

Uncorrelated initial conditions are considered: at time $t = 0$ every site is occupied with the same probability p. In this case:

$$B^{-1}|\vec{P}_0\rangle = \begin{pmatrix} 1 - \frac{\hat{a}+\hat{f}}{\hat{a}+2\hat{f}}p \\ \frac{\hat{a}+\hat{f}}{\hat{a}+2\hat{f}}p \end{pmatrix}_1 \otimes \cdots \otimes \begin{pmatrix} 1 - \frac{\hat{a}+\hat{f}}{\hat{a}+2\hat{f}}p \\ \frac{\hat{a}+\hat{f}}{\hat{a}+2\hat{f}}p \end{pmatrix}_L$$

which corresponds to an initial site occupation probability in the equivalent annihilation model equal to $\frac{\hat{a}+\hat{f}}{\hat{a}+2\hat{f}}p$.

The operator of the occupation number of the site i is given by:

$$n_i = \left(\begin{array}{cc} 0 & 0 \\ 0 & 1 \end{array} \right)_i . \tag{4.2.5}$$

The expectation value of the product of k such operators in the coagulation-annihilation model is (4.1.3):

$$< n_{i_1} \widehat{\cdots} n_{i_k} >(p,t) = \left(\frac{\hat{a}+2\hat{f}}{\hat{a}+\hat{f}} \right)^k < n_{i_1} \cdots n_{i_k} >_{\text{ann.}} \left(\frac{\hat{a}+\hat{f}}{\hat{a}+2\hat{f}}p, t \right) \tag{4.2.6}$$

We now drop the superscript.

The exactly solvable case $\Delta' = 1 - f - \frac{a}{2} = 0$ corresponds to the physical situation that whenever two particle meet at least one of them disappears from the system. We mentioned in the introduction that the operators which appears in the master equation of these models are the Hamiltonians of supersymmetric systems. This reaction-diffusion models are mentioned in [32] in connection with the Glauber dynamic of the q state Potts model. The results given in [13] for $f = 1$ or $a = 2$ can be generalized to these annihilation-coagulation models. The particle concentration on a finite chain is:

$$\begin{aligned} c(t,p,L) &= \frac{1 - [1-(2-f)p]^L}{(2-f)\,L} \\ &- \frac{1}{(2-f)\,L} \sum_{k=1}^{L-1} \left\{ \left[\frac{1-(-1)^k[1-(2-f)p]^L}{\frac{1+[1-(2-f)p]^2}{2[1-(2-f)p]} - \cos\frac{\pi k}{L}} - \frac{1-(-1)^k[1-(2-f)p]^L}{1-\cos\frac{\pi k}{L}} \right] \right. \\ &\left. \times \sin^2\left(\frac{\pi k}{L}\right) \exp\left[-4t\left(1 - \cos\frac{\pi k}{L}\right)\right] \right\} . \end{aligned} \tag{4.2.7}$$

The behavior of the concentration (4.2.7) in the finite-size scaling limit [2]:

$$L \to \inf, \quad t \to \inf \quad \text{with} \quad z' = \frac{4t}{L^2} \quad \text{fixed} \tag{4.2.8}$$

can be determined [13]. Exact expressions can be written for the scaling and the first correction functions in terms of Jacobi theta functions. We get the following scaling relation:

$$\begin{aligned} L\,c(z',p,L) &= \frac{1}{2-f}\left\{ \theta_3\left(0, \frac{i\pi z'}{2}\right) + \frac{1}{L^2}\left[\frac{z'}{6}\frac{\partial^2}{\partial z'^2}\theta_3\left(0,\frac{i\pi z'}{2}\right) \right.\right. \\ &\left.\left. + \frac{1}{2}\left(1 - \frac{2}{(2-f)p}\right)^2 \frac{\partial}{\partial z'}\theta_3\left(0,\frac{i\pi z'}{2}\right)\right] \right\} + O\left(\frac{1}{L^4}\right). \end{aligned} \tag{4.2.9}$$

Another interesting result concerns the large time behavior of the particle concentration in the thermodynamic limit. In the $\Delta' \neq \emptyset$ case we start from the conjectured expression (4.0.2). Applying (4.1.3) we get:

$$c(t) = \frac{a+2f}{a+f}\left[\sqrt{\frac{1}{8\pi t}} + \frac{R}{2\pi}\frac{\Delta'}{1-\Delta'}\frac{1}{t} \right] + O(t^{-x}) \tag{4.2.10}$$

The coefficient of the leading term depends only on the ratio of the annihilation and the coagulation rates. The next to leading term ($\sim \frac{1}{t}$) is dependent of Δ'. Both of them are independent on the initial concentration. We will give strong numerical evidence which supports the conjecture presented in [39] (i.e. $R = 1$) in Section (4.3).

This asymptotic expression is an exact result in the supersymmetric ($\Delta' = 0$) case [7]. The next to leading term is of order $t^{-3/2}$. For uncorrelated homogeneous initial conditions, in the $z' \to \emptyset$ limit [13] of (4.2.9) one gets:

$$
\begin{aligned}
c(t,p) \; = \; & \frac{1}{2-f}\Bigg\{\sqrt{\frac{1}{2\pi t}} \\
& -\frac{1}{\sqrt{2\pi}}\frac{1}{16}\left[\left(1-\frac{2}{(2-f)p}\right)^2-\frac{1}{2}\right]\frac{1}{t^{3/2}}\Bigg\} + O(t^{-5/2})
\end{aligned}
\tag{4.2.11}
$$

We return now to the *coagulation-diffusion model with particle input at the endpoints of the lattice* as it was defined in Chapter 3. That model isn't, in generally, left-right symmetric. That is why we return to the general notation of the rates given in the Introduction.

The transformation (4.2.1) can be used in order to generalize the results of that chapter to a coagulation-annihilation model (called CA) with boundary effects. It's hamiltonian

$$
\hat{H}^{CA} = \hat{h}_1^{CA} + \hat{h}_L^{CA} + \sum_{n=1}^{L-1} \hat{H}_{n,n+1}^{CA}
$$

is obtained from the hamiltonian H defined by equations (3.0.1-3.0.3)

$$
\hat{H}^{CA} = BHB^{-1}
$$

The processes allowed in the bulk define $\hat{H}^{CA}_{n,n+1}$. Their rates are

$$
\begin{aligned}
\hat{\Gamma}^{01}_{10} &= \Gamma^{01}_{10} \\
\hat{\Gamma}^{10}_{01} &= \Gamma^{10}_{01} \\
\hat{\Gamma}^{11}_{10} &= \Gamma^{11}_{10} + \frac{\beta}{1-\beta}(\Gamma^{10}_{01} - \Gamma^{01}_{10} - \Gamma^{11}_{01}) \\
\hat{\Gamma}^{11}_{01} &= \Gamma^{11}_{01} + \frac{\beta}{1-\beta}(\Gamma^{01}_{10} - \Gamma^{10}_{01} - \Gamma^{11}_{10}) \\
\hat{\Gamma}^{11}_{00} &= \frac{\beta}{1-\beta}(\Gamma^{11}_{01} + \Gamma^{11}_{10})
\end{aligned}
\tag{4.2.12}
$$

The diffusion rates in the two models are equal. In the generalized model, particle can coagulate and also annihilate. The positivity of the rates of the transformed model implies that $1/2 \leq \beta \leq 1$ and $\Gamma^{11}_{10} + \beta(\Gamma^{10}_{01} - \Gamma^{01}_{10} - \Gamma^{11}_{01} - \Gamma^{11}_{10}) \geq 0$.

In addition particles are absorbed and desorbed at the boundaries. The rates defining $\hat{h}_1^{CA}$ and $\hat{h}_L^{CA}$ are

$$
\begin{aligned}
\hat{\Gamma}^{01}_{l} &= (1-\beta)p_l \\
\hat{\Gamma}^{10}_{l} &= \beta p_l \\
\hat{\Gamma}^{01}_{r} &= (1-\beta)p_r \\
\hat{\Gamma}^{10}_{r} &= \beta p_r
\end{aligned}
$$

Notice that if the original model had only input of particles the equivalent coagulation-annihilation model has both input and output of particles.
Because of the simplicity of the transformation the n-point density-density correlation functions in the coagulation and coagulation-annihilation model are related by

$$\langle \tau_{j_1}\tau_{j_2}\ldots\tau_{j_n}\rangle^{CA} \;=\; (1-\beta)^n \, \langle \tau_{j_1}\tau_{j_2}\ldots\tau_{j_n}\rangle^{coag} \tag{4.2.13}$$

The left-right symmetric coagulation-decoagulation model. In this system, apart from diffusion, coagulation and its backward reaction are permitted. We will use, as in [13], the variable η defined through the decoagulation rate: $\eta^2 \;=\; \Gamma_{11}^{10}+1$.

Exact solutions of this model are available in the continuum limit [10] and for the finite lattice in the case in which the coagulation and diffusion rates are equal ($f=1$) [13]. In the latter case the steady state concentration is $c_s = 1-\eta^{-2}$, independently of L and p.

We found that the coagulation-decoagulation model is equivalent with two other reaction-diffusion systems. Only two transformations, which correspond to special choices for α and β in (4.2.1), connect this model with others.

a) One of them is:

$$b = \begin{pmatrix} 1 & -\frac{f}{\eta^2-1} \\ 0 & 1+\frac{f}{\eta^2-1} \end{pmatrix} \tag{4.2.14}$$

If $f\leq 1$, the transformed Hamiltonian $\hat{H}$ corresponds to a reaction-diffusion system with the following processes:

- diffusion with rate $\hat{\Gamma}_{01}^{10} \;=\; 1-f$
- decoagulation with rate $\hat{\Gamma}_{11}^{10} \;=\; f+\eta^2-1$
- death with rate $\hat{\Gamma}_{00}^{10} \;=\; f$

If $f=1$ there is no diffusion in the new model. The motion of the particles is realized by successive processes of decoagulation (with rate $\eta^2 > 1$) and death (with rate 1) on neighboring pairs of lattice sites. In this case we can use the results from [13]. For the finite chain and homogeneous random initial conditions the particle concentration is:

$$\begin{aligned} c(t,p,L) \;&=\; \frac{1-[1-p(1-\eta^{-2})]^L}{1-\eta^{-2L}} \\ &- \frac{1}{\eta L}\sum_{k=1}^{L-1}\left\{\left[\frac{1+(-1)^{k+1}\eta^L[1-p(1-\eta^{-2})]^L}{\frac{1+\eta^2[1-p(1-\eta^{-2})]^2}{2\eta[1-p(1-\eta^{-2})]}-\cos\frac{\pi k}{L}} - \frac{1+(-1)^{k+1}\eta^L[1-p(1-\eta^{-2})]^L}{\frac{\eta^2+1}{2\eta}-\cos\frac{\pi k}{L}}\right]\right. \\ &\left.\times\, \sin^2\left(\frac{\pi k}{L}\right)\exp\left(-\Lambda_k^0 t\right)\right\}. \end{aligned} \tag{4.2.15}$$

where Λ_k^0 is:

$$\Lambda_k^0 = \eta\Big(2(\eta+\eta^{-1}) \;-\; 4\,\cos\frac{\pi k}{L}\Big)\,. \tag{4.2.16}$$

The full lattice is a stationary state:

$$c(0,1,L) \;=\; c(t,1,L) \;=\; 1.$$

Interchanging A and $\emptyset$ a system with a death rate η^2 greater than the decoagulation rate 1 and zero steady state concentration is obtained. For this choice of rates (4.2.15) gives the concentration of vacancies if p is replaced by $1-p$.

b) The other transformation which gives a mapping of the coagulation-decoagulation model is:

$$b = \begin{pmatrix} \frac{1}{2}\left[1+\sqrt{\frac{\eta^2-1}{f}+1}\right] & \frac{1}{2} \\ \\ \frac{1}{2}\left[1-\sqrt{\frac{\eta^2-1}{f}+1}-1\right] & \frac{1}{2} \end{pmatrix} \tag{4.2.17}$$

One obtains an annihilation-creation reaction-diffusion system with rates:

- diffusion $\hat{\Gamma}^{10}_{01} \;=\; \frac{\eta^2+1}{2}$
- annihilation $\hat{\Gamma}^{11}_{00} \;=\; \hat{a} \;=\; \frac{1}{2}\left[\sqrt{\frac{\eta^2-1}{f}+1}+1\right]^2 f^2$
- creation $\hat{\Gamma}^{00}_{11} \;=\; \frac{1}{2}\left[\sqrt{\frac{\eta^2-1}{f}+1}-1\right]^2 f^2.$

The annihilation rate is greater than the creation rate. The time unit can be adjusted in such a way that the new diffusion rate $\hat{\Gamma}^{10}_{01}$ becomes equal to 1.

In the case $f=1$ the sum of the annihilation and creation rates is equal to 2. We can redefine the variable η:

$$\eta = 1 + \frac{2}{\left(\frac{\hat{a}}{2-\hat{a}}\right)^y - 1}$$

where $y = 1/2$. The concentration for the finite chain is:

$$\begin{aligned} c(t,p,L) \;\;&=\;\; \frac{1-\eta}{2} + \frac{(\eta-\eta^{-1})[1-(1-2p)^L\eta^{-L}]}{2(1-\eta^{-2L})} \\ &\quad - \frac{1}{2L}\sum_{k=1}^{L-1}\left\{\left[\frac{1+(-1)^{k+1}(1-2p)^L}{\frac{1+(1-2p)^2}{2(1-2p)}-\cos\frac{\pi k}{L}} - \frac{1+(-1)^{k+1}(1-2p)^L}{\frac{\eta^2+1}{2\eta}-\cos\frac{\pi k}{L}}\right]\right. \\ &\quad \left. \times \sin^2\left(\frac{\pi k}{L}\right)\exp\left(-\Lambda^0_k t\right)\right\}. \end{aligned} \tag{4.2.18}$$

where Λ^0_k is:

$$\Lambda^0_k = \frac{2\eta}{\eta^2+1}\left(2(\eta+\eta^{-1}) \;-4\;\cos\frac{\pi k}{L}\right). \tag{4.2.19}$$

The steady-state concentration is $c_s = (1-\eta^{-1})/2 \;<\; 0.5$.

After a permutation of the two lines in (4.2.17) a system with interchanged annihilation and creation rates is obtained. The redefinition of η in the exactly solved case is the same as the one given above but with $y = -1/2$. Formula (4.2.18) gives the vacancies concentration if p is again replaced with $1-p$. The steady-state concentration is $c_s = (1+\eta^{-1})/2 > 0.5$.

In the limit $\eta \to \inf$ the reaction-diffusion system in which all three rates are equal is obtained. The operator which appears in the corresponding master equation is the Hamiltonian of the Ising model [2].

4.2.2 Three state models

The starting point in this section is the two-species annihilation model. The particles diffuse and react when an A and a B try to occupy the same site:

$$A + B \longrightarrow \emptyset + \emptyset.$$

We denote the annihilation rate with a ($\Gamma^{12}_{00} = a$), as in the preceding section. All diffusion rates are equal to 1 and $\Gamma^{21}_{12} = 0$ modeling a hard-core interactions between particles.

The two sites Hamiltonian for this model is given by:

$$H = 2 \times \begin{pmatrix} 0 & 0 & 0 & 0 & 0 & -a & 0 & -a & 0 \\ 0 & 1 & 0 & -1 & 0 & 0 & 0 & 0 & 0 \\ 0 & 0 & 1 & 0 & 0 & 0 & -1 & 0 & 0 \\ 0 & -1 & 0 & 1 & 0 & 0 & 0 & 0 & 0 \\ 0 & 0 & 0 & 0 & 0 & 0 & 0 & 0 & 0 \\ 0 & 0 & 0 & 0 & 0 & a & 0 & 0 & 0 \\ 0 & 0 & -1 & 0 & 0 & 0 & 1 & 0 & 0 \\ 0 & 0 & 0 & 0 & 0 & 0 & 0 & a & 0 \\ 0 & 0 & 0 & 0 & 0 & 0 & 0 & 0 & 0 \end{pmatrix} \tag{4.2.20}$$

in the $\{|00\rangle,\ |01\rangle,\ |02\rangle, \cdots |22\rangle\}$ base.

A general transformation has the form (4.1.6):

$$b = \begin{pmatrix} 1-\alpha-\beta & \gamma & \epsilon \\ \alpha & 1-\gamma-\delta & \zeta \\ \beta & \delta & 1-\zeta-\epsilon \end{pmatrix} \tag{4.2.21}$$

We have to insure that the transformed Hamiltonian satisfies the condition (4.1.7). The first, fifth and ninth columns of $\hat{H}$ are identical up to a factor. So are the line one, five and nine. The matrix elements of $\hat{H}$ can be interpreted in terms of reaction rates only if the entries from at least one of these lines or from its corresponding column are zero. The other two lines $i, j \in \{1,5,9\}$ have at most two non-zero entries in the two corresponding columns i, j. By imposing this conditions we are left with one transformation:

$$b = \begin{pmatrix} 1 & 1-\alpha & 1-\beta \\ 0 & \alpha & 0 \\ 0 & 0 & \beta \end{pmatrix} \tag{4.2.22}$$

which leads to a new reaction-diffusion system if a ,α and β are greater than one and if $\alpha^{-1}+\beta^{-1} \geq 1$. The transformed two sites Hamiltonian is:

$$\hat{H} = 2 \times \begin{pmatrix} 0 & 0 & 0 & 0 & 0 & -a(-1+\alpha^{-1}+\beta^{-1}) & 0 & -a(-1+\alpha^{-1}+\beta^{-1} & 0 \\ 0 & 1 & 0 & -1 & 0 & -(1-\alpha^{-1}) & 0 & -(a-1)(1-\alpha^{-1}) & 0 \\ 0 & 0 & 1 & 0 & 0 & -(a-1)(1-\beta^{-1}) & -1 & -(1-\beta^{-1}) & 0 \\ 0 & -1 & 0 & 1 & 0 & -(a-1)(1-\alpha^{-1}) & 0 & -(1-\alpha^{-1}) & 0 \\ 0 & 0 & 0 & 0 & 0 & 0 & 0 & 0 & 0 \\ 0 & 0 & 0 & 0 & 0 & a & 0 & 0 & 0 \\ 0 & 0 & -1 & 0 & 0 & -(1-\beta^{-1}) & 1 & -(a-1)(1-\beta^{-1}) & 0 \\ 0 & 0 & 0 & 0 & 0 & 0 & 0 & a & 0 \\ 0 & 0 & 0 & 0 & 0 & 0 & 0 & 0 & 0 \end{pmatrix} \quad (4.2.23)$$

$\hat{H}$ has the same diffusion part and is left-right symmetric. All processes which reduce the number of particles start from a $A\,B$ pair. Apart from annihilation we have 'two species coagulation' reactions:

- $A + B \to \emptyset + \emptyset$ with rate $\hat{\Gamma}^{12}_{00} = a\,(\alpha^{-1}+\beta^{-1}-1)$
- $A + B \to \emptyset + A$ with rate $\hat{\Gamma}^{12}_{01} = 1-\alpha^{-1}$
- $A + B \to A + \emptyset$ with rate $\hat{\Gamma}^{12}_{10} = (a-1)(1-\alpha^{-1})$
- $A + B \to B + \emptyset$ with rate $\hat{\Gamma}^{12}_{20} = 1-\beta^{-1}$
- $A + B \to \emptyset + B$ with rate $\hat{\Gamma}^{12}_{02} = (a-1)(1-\beta^{-1})$

Note that the diagonal terms of the Hamiltonian are invariant under the transformation ($\hat{\Gamma}_{12} = \Gamma_{12} = a$). The coagulation rates depend on the type of the particle which survives the process and they are $(a-1)$ times smaller if the particle which survives is the one which jumps. There are only two coagulation rates, independent of the initial position of the surviving particle if $a = 2$. This case corresponds to the physical situation in which at any A B encounter at least one particle leaves the system.

From (4.1.3) and (4.0.3) it is easy to see that the concentration will have an algebraic fall-off if:

$$\frac{c_A(0)}{c_B(0)} = \frac{\alpha}{\beta}.$$

In this case the particle concentrations are:

$$c_A(t) = \alpha^{\frac{1}{2}} \frac{K'\sqrt{c_A(0)}}{t^{1/4}} \quad (4.2.24)$$

$$c_B(t) = \beta^{\frac{1}{2}} \frac{K'\sqrt{c_B(0)}}{t^{1/4}} = \frac{\beta}{\alpha} c_A(t) \quad (4.2.25)$$

4.3 Monte Carlo Simulations

Only a few chemical models have been solved exactly. For some others, quantitative estimates have been made with the help of approximation schemes. This is the reason why numerical methods have been extensively used in the study of reaction-diffusion systems. The dynamics of the particle density and spatial distribution can be determined with the help of Monte Carlo simulations [46, 8].

The Hamiltonian formalism opens new possibilities in this field. For small chains numerical data can be obtained with a high accuracy by using diagonalization techniques or simulations. The study of the finite-size scaling behavior (4.2.8) in the limit $z' \to \emptyset$ permits the determination of the particle concentration for infinite chains at very large times [45].

In this section we present our numerical results concerning the asymptotic behavior of the particle concentration in the one and two species annihilation models. We simulate directly the thermodynamical limit by using large lattices.

We consider chemical systems in which no reaction is permitted which creates particles on a pair of empty sites. This is why the so called 'direct' Monte Carlo Method [46, 47] can be used. The way we implement this method is described in detail in [45].

We will first present our results for the two state models and continue with the three state models.

4.3.1 The two state annihilation-coagulation model

The influence of the reaction rate in annihilation and coagulation models is a subject which has received a lot of attention in recent years (see [38, 39] and references therein). We mentioned in the introduction the conjectured expression (4.0.2) for the concentration decay in the $\Delta' \neq \emptyset$ coagulation model. This result is in agreement with the conclusions of a numerical study we carried out in our previous work. Using a finite-size scaling analysis we obtained the same value for the time exponents in the leading $(-1/2)$ and the next to leading term (-1) and we found that the coefficient of the leading term is independent of Δ' [45].

As mentioned there, a better test of (4.0.2) (or equivalently of (4.2.10)) can be made through a direct simulation of the thermodynamic limit. Results of such computations are presented in [39]. They are, in some cases, in semi-quantitative agreement with the conjecture presented there. We concentrate on the long time behavior and use smaller lattices as the one mentioned in [39]. Thus we are able to obtain very good statistic in a reasonable CPU time.

We tested the conjecture (4.0.2) in two different ways. Simulations of the annihilation model were performed on a lattice of length $L = 2000$ for times up to a value of $t_{max} = 1.5 \times 10^4$.

In the first set of simulations two values for the initial concentrations, 1.0 and 0.1, were used. A decrease of 3 respectively 2 orders of magnitude of the concentration enables us to reach the asymptotic regime. 300,000 runs were performed in order to insure a relative error of the particle concentration of less then 10^{-3}. In Figure 4.1[2] the following quantity (see (4.2.10) with $f = 0$):

$$R(t) = 2\pi \left(c(t) - \sqrt{\frac{1}{8\pi t}} \right) \frac{1 - \Delta'}{\Delta'} t \tag{4.3.1}$$

is represented for $\Delta' = 0.875$ and 0.75. We see that our data converges to the value $R(t) = 1$ for which the straight line is drawn.

[2] The Monte Carlo data are represented by interrupted lines. Error bars are given only for a few points.

Δ'	Initial concentration $c(0)$	Values of R from M.C. data
-7	1.00	1.090 ± 0.020
-7	0.10	1.060 ± 0.010
$-3/2$	1.00	0.940 ± 0.010
$-27/28$	1.00	0.950 ± 0.020
-1	1.00	1.000 ± 0.040
-1	0.25	1.180 ± 0.080
-1	0.10	1.060 ± 0.080
$-3/7$	1.00	1.010 ± 0.030
$-1/9$	1.00	0.940 ± 0.070
$1/2$	1.00	1.060 ± 0.040
$1/2$	0.25	0.990 ± 0.040
$3/4$	1.00	1.004 ± 0.005
$3/4$	0.10	1.030 ± 0.020
$7/8$	1.00	0.998 ± 0.005
$7/8$	0.10	1.005 ± 0.005

Table I: Values of R (4.0.2) obtained from Monte Carlo simulations of the annihilation model. The two different conjectured values are 1 [39] and 0.786 [38]

Simulations were also performed for negative values of Δ'. The convergence is worse, $R(t)$ seems to oscillate. In this case the absolute value of the next to leading term of (4.2.10) is smaller than for positive Δ's, so $R(t)$ approaches faster the order of magnitude of the numerical errors.

A second set of simulations of the annihilation model were performed in which we averaged only over 20,000 runs. We applied a χ^2 test in two steps to the data. A linear combination of time powers was presumed:

$$y \;=\; K_x t^{-x} \;+\; K_{x+1/2} t^{-x-1/2} \;+\; K_{x+1} t^{-x-1} \tag{4.3.2}$$

The first fit was made for the concentration $y = c(t)$ taking $x = 1/2$. The coefficient of the leading term was determined with a confidence level greater then 99%. The first three significant digits of $K_{1/2}$ are identical with those of $(8\pi)^{-1/2} \simeq 0.1995$.

The next step is to determine the coefficient of the first correction. The leading term is subtracted from the numerical data:

$$y \;=\; c(t) \;-\; \frac{1}{\sqrt{8\pi t}}$$

and a value $x = 1$ is used in the fit (4.3.2). The confidence level was good (greater then 50%). The values for R are listed in table I.

For most values of Δ' simulations of the same model with different initial concentrations were performed, as can be seen in table I. The best fits were obtained for the choice of reaction rates corresponding to a value of Δ' near 1. This is easy to understand because for such Δ's the contribution of the next to leading term in (4.2.10) is maximal. The simulations corresponding to $\Delta' = 3/4$, and 7/8 are the ones used to make Figure 4.1. For this data the statistic was made by averaging over 300,000 runs.

The conclusion we draw from the results of the two tests is that the conjecture presented in [39], predicting a value of $R = 1$ in (4.0.2) is correct.

This results are valid if the data we considered before are not affected by the finite size of the lattice on which the simulations were performed. We check this by performing the simulations described in the following.

In the asymptotic regime the system contains a low number of particles which are spatially separated. A particle which was not involved in a reaction represents a random walker. This means that at large times, of the order of the square of lattice length, finite-size effects should be dominant.

We obtain a more precise quantitative picture from simulations of the annihilation model for times up to $t_{max} = 10^6$. We use a lattice of the same length ($L = 2,000$) and averaged over 20,000 runs. Three values for the parameter Δ' were chosen: $7/8$, 0 and -7 . Each simulation started with a full lattice as initial configuration.

For an infinite system the long time behavior of the concentration is algebraic .

For a finite system the concentration decay is exponential. We are interested to study the transition between the two types of decay, i.e. the onset of finite size effects at large times.

Figure 4.2 gives a log-log plot of the concentration. The straight line corresponds to $c(t) = (8\pi t)^{-1/2}$. We see that for times $t > 10^5$ the dashed lines strongly deviate from the straight line.

In Figure 4.3 which is a plot of the logarithm of the concentration we can see that starting from the same value of time ($t = 10^5$) the curves fit nicely with another straight line described by:

$$c(t) = \frac{2}{L} \exp\left(-2\,\frac{\pi^2}{L^2}t\right) . \tag{4.3.3}$$

The formula is obtained in the $t \to \inf$ limit of (4.2.7), for the $\Delta' = 0$ annihilation model ($c = 0$).

From Figures 4.2 and 4.3 we conclude that the onset of the finite-size effects takes place in a narrow vicinity of $t = 10^5$. This value is considerably smaller than L^2 but much larger than the t_{max} we used. It is now clear that the results we presented in the first part of this section refer to the thermodynamic limit of the annihilation model.

The slope of the line from Figure 4.3 is equal to the energy of the first excited state of $H_{\text{ann.}}$. We can conclude that this energy has the value $4(1 - \cos(\pi/L))$ independent of the parameter Δ'. This confirms previous results obtained from numerical diagonalization of this Hamiltonian [48].

4.3.2 Numerical results for the three state models

The simulation of the thermodynamic limit of the two species annihilation reaction requires a very large amount of *CPU* time.

This has two reasons. A reliable study of the long time decay of the concentration presumes simulations in which the total number of particles reduces by at least two orders of magnitude. The algebraic fall-off is much slower than in the $A + A \longrightarrow \emptyset + \emptyset$ case. This means that we have to perform the simulations up to much higher values of t_{max} than we did in the one species case.

On the other hand, if we start at $t = 0$ with a random distribution, there will be local fluctuations of the particle densities. The decay of the initial fluctuations plays an essential role in the dynamics of the system [42]. Their length scale extends in time. So one is forced to use longer lattices than in the one-species case where such domains do not appear.

A lattice of length $L = 10^5$ was used to simulate three state models. In the case of the two species annihilation we were able to average only over 100 runs. We have chosen small values of the initial density, as suggested by the results obtained for the $d = 2$ case [43]. Our aim is to see if the particle concentration obeys the algebraic decay law (4.0.3) for the $A - B$ symmetric case and to compute K'. Results from similar simulations were reported in [42] which lead to $K' = 0.280$. This is in equally good agreement with the two conjectured values 0.252 and 0.316.

Figure 4.4 shows the curve

$$K(t) \;=\; c_A(t)\,\frac{t^{1/4}}{\sqrt{c(0)}} \tag{4.3.4}$$

for various choices of the annihilation rate and initial site occupation probabilities. The simulations were stopped at values of t_{max} of the order of 10^6.

These values of t_{max} are a hundred times larger as the one used in [42]. At very large times the asymptotic regime is reached with the three curves converging to slightly different values. However the difference between the limit values is less than the sum of their standard deviations.

Our data show a weak dependence of $K(t)$ on a and $c(0)$. This suggests that K' in (4.0.3) is a function of these parameters. This may well not be the case because the next to leading terms in the asymptotic development of the concentration also contribute to $K(t)$ and can determine the difference between the three curves.

We get the estimate $K' = 0.251 \pm 0.003$ by averaging over the three limit values. Our result is important because it shows that the conjectured dependence of the concentration on its initial value [42] is most probably correct.

The weak dependence of $K(t)$ on a suggests that the asymptotic behavior is universal in the sense it is independent of the annihilation rate. For a better numerical confirmation one should apply the procedure described in the previous section for the $A + A \longrightarrow \emptyset + \emptyset$ case. The first step would be to determine the exponent x in (4.0.3) [45] and then apply χ^2 tests. This would require a better statistics in the determination of the asymptotic behavior of the concentration. This is an aim which we cannot achieve with the computer facilities which are currently at our disposal.

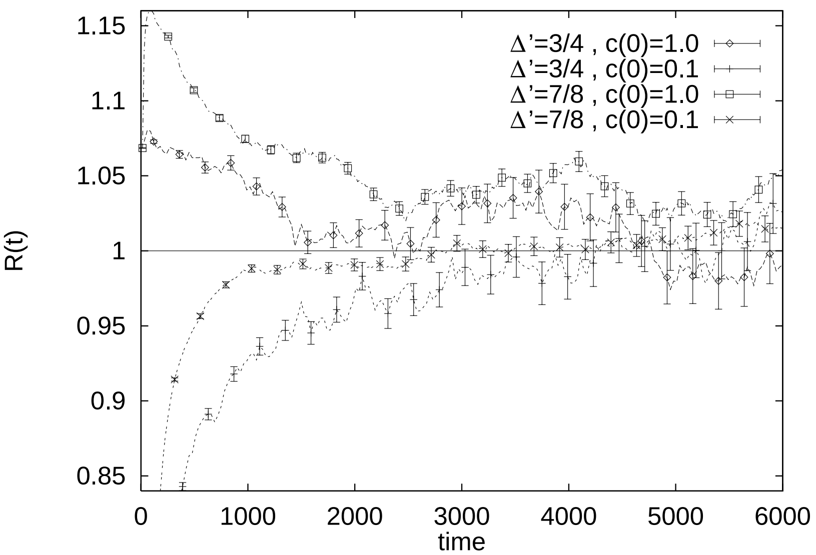

Figure 4.1: Effects of the annihilation rate on the asymptotic behavior of the particle concentration for the $A + A \longrightarrow 0 + 0$ reaction $-$ $R(t)$ as defined by (4.3.1), for $\Delta' = 3/4$ and $7/8$. The straight line is $R(t) = 1$.

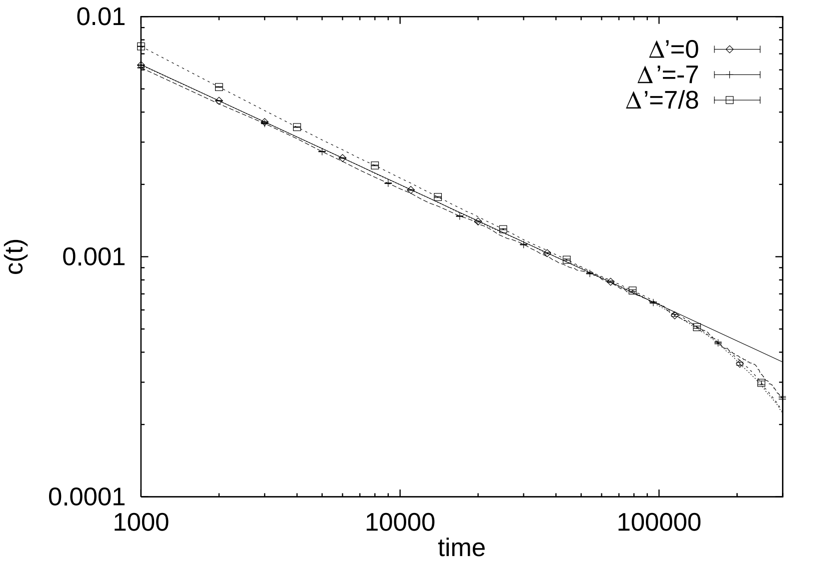

Figure 4.2: Onset of finite size effects - the algebraic decay. Double logarithmical plot of the concentration for the one-species annihilation reaction.

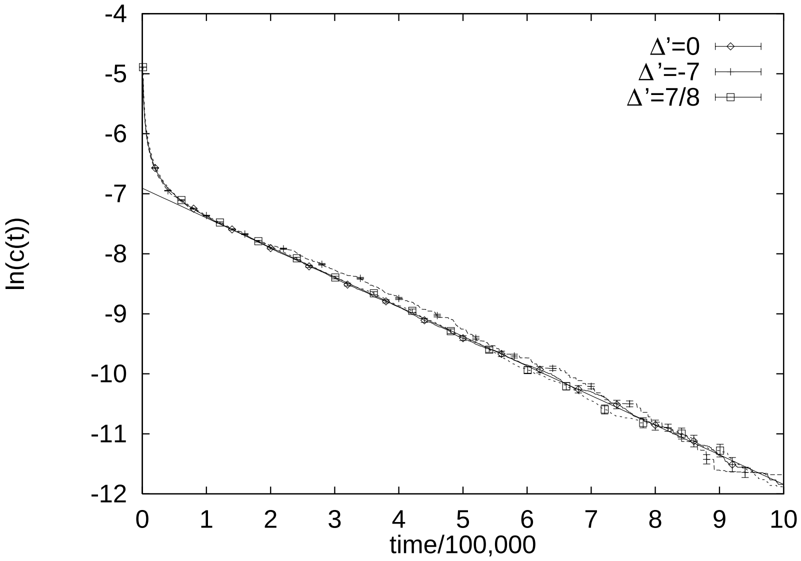

Figure 4.3: Onset of finite size effects - the exponential decay. Plot of the logarithm of the concentration for the one-species annihilation reaction.

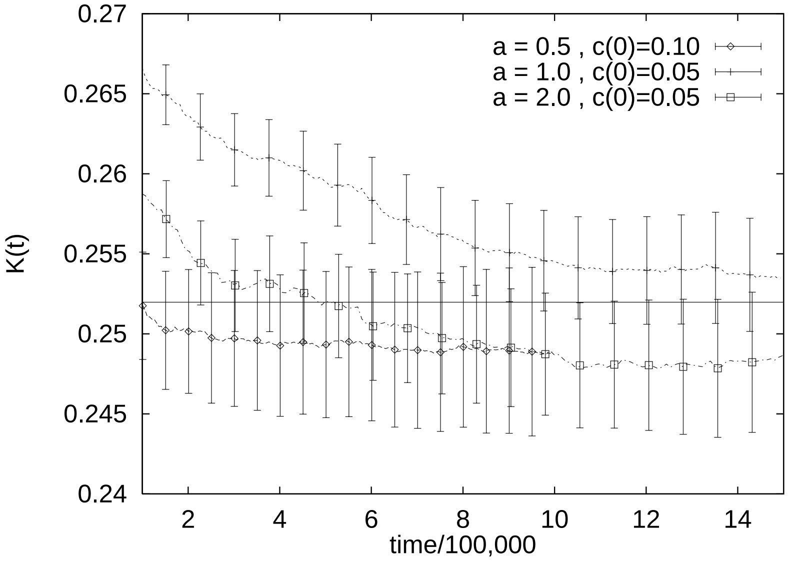

Figure 4.4: Asymptotical behavior of the particle concentration in the $A + B \longrightarrow 0 + 0$ reaction. Plot of $K(t)$ as defined by (4.3.4). The straight line corresponds to $K(t) = (2\pi)^{-3/4}$)

Chapter 5

Conclusions

In **Chapter 2** the mean field computations for the fully asymmetric exclusion model are presented. A current with no divergency can be defined, due to the fact that particle can only diffuse in the bulk. We determined the density profile and the particle current in the steady state in the thermodynamical limit. The phase diagram can be drawn by using mean field results. The dependence of the current on the input and output rates is confirmed by the exact solution. With the exception of the coexistence line, the mean field computations give the correct nature (exponential or algebraic) of the density decay in the different phases. Universality properties of the density are also a common feature of the exact and mean field solution. The mean field picture is not complete. The exponent of the massless and the correlation lengths of the massive phases are not correctly determined. This is reflected in the fact that there are transition lines which are not captured in the mean field description.

The same kind of conclusion can be drawn after the comparison of the mean field with the exact solutions of the model presented in Chapter 3. It would be interesting to learn up to which extend one can use the mean field predictions in the case of one-dimensional systems with particle input and output at its ends. This remains an open question.

In **Chapter 3** we investigated the coagulation-diffusion model with particle input at one boundary using both analytical and numerical methods. The results show that spatial long-range correlations play an essential role and that some physical properties are universal with respect to the input and the coagulation rates.

We started our analysis with a simple space-dependent mean field approximation. It predicts algebraic behavior of the particle density in the stationary state for both symmetric and biased diffusion. However, rigorous results require an exact solution of the problem. To this end we solved the full problem by using the IPDF formalism. This formalism can be used only if the coagulation rates coincide with the diffusion rates, which corresponds to free fermions in the Hamiltonian language. The large x behavior (x is the distance to the source) of the particle density was computed in the thermodynamical limit both for the lattice and the continuum version and the results are compared. These painful calculations were done for symmetric and asymmetric diffusion. In the case of symmetric diffusion the scaling limit (x/L fixed, L is the lattice length) was obtained.

Monte Carlo simulations show that the coefficient of the leading terms of the asymptotic expansion of the density in the thermodynamical limit are universal: they are independent of the input rates (this was to be expected from mean-field) and on the coagulation rates. The scaling function is also universal in the symmetric case. It is trivial in the asymmetric case (it coincides with the leading term of the large x behavior of the density). These results were to be expected from common sense in the symmetric case but not for the asymmetric case. The reason is the following one: the relaxation spectrum of the system is massless in the first but massive in the second case. There exists a myth according to which if there are lengths in the time evolution there should be lengths in the space correlations. A counter-example can be found however in the kinetic Ising model (see Ref. [2]). In the coagulation-diffusion model the picture is more perverse : if one looks at the concentration starting at the opened end, one finds an exponential fall-off but an algebraic and universal behavior if we start at the source end.

The message of this study can be extended to the problem in which we add pair-annihilation in the bulk and an output of particles at the source. What is still missing is a proof of universality which goes beyond numerical checks. This can be done using field theoretical methods à la Cardy [49, 50].

In the **Chapter 4** we found a general condition satisfied by local transformations which realize mappings between reaction-diffusion systems. They are $N \times (N-1)$-parameter real matrices which have the sum of entries in each column equal to one.

Some new results concerning two state models are derived:

All annihilation-coagulation systems corresponding to the same parameter Δ' (4.2.3) are equivalent. The continuous similarity transformation which acts between these models is given. Results previously derived for the coagulation and annihilation models are generalized to the chemical systems in which both reactions are permitted.

At this point we return to the exciton decay measurements mentioned at the beginning of chapter 4. Further experimental determinations are very desirable for two reasons:

1) It would be interesting to have accurate measurements of the exciton hopping time which is related to their diffusion constant. The coefficient of the leading term ($\sim t^{-1/2}$) in the exciton concentration decay can then be extracted from the experimental data [37]. Thus one can determinate the ratio of the exciton-exciton annihilation and coagulation rates(4.2.10).

2)Lower errors in the experimental measurements of the luminescence decay would permit the computation of the next to leading term (its time exponent and coefficient) which appears in an expansion of the exciton concentration.

If this term is of order $t^{-3/2}$ (4.2.11) the dynamic of exciton propagation and reactions is described by a system which is supersymmetric [2]. This would be the first such system experimentally measured. The other possibility is that the next to leading term is of order t^{-1} (4.2.10). In both cases the determination of the leading and next to leading term and of the hopping time would permit the computation of the rates of the processes which take place between excitons.

The two states coagulation-decoagulation, annihilation-creation and death-decoagulation models are equivalent. This enables us to give an exact expression for the particle number for a non-diffusive driven, death-decoagulation system. The same observable is computed for the model in which the sum of the annihilation and creation probabilities is one (4.2.18).

A reaction-diffusion system equivalent to the two species annihilation ($A+B \to \emptyset+\emptyset$) is found.

We have accurately determined the effect of the reaction rate on the long time decay of the concentration in the one-species annihilation model. Our results are in excellent agreement with a theoretical conjecture previously made in [39].

We also present quantitative analysis of the asymptotic behavior of concentration in the three states annihilation model. Results of simulations performed for different values of the rate of the $A + B \longrightarrow \emptyset + \emptyset$ reaction are presented. They are fully compatible with previous results.

Chapter 6

Acknowledgments

This work could not have been finalized without the warm support and advice (covering not only topics from physics) of Prof. Vladimir Rittenberg.

I thank my wife Gudrun for her fully and unconditional support and for believing in me.

I thank my parents for understanding and encouraging me. I am much in debt to Prof. Ion I. Cotăescu from the University of Timisoara, a man who has been for many years my mentor. I would also like to thank Professors Otto Aczel and Emeric Hegedüs for passionately teaching me physics.

My colleages Peter Arndt & Thomas Heinzel, Ulrich Bilstein, Markus Pfannmüller, Birgit Wehefritz and Thomas Wittlich helped me a lot with friendly advices and encouradgement. Some of the nicest moments I spended in Bonn were those by "Sam". Special thanks go to Silvio Renato Dahmen for sharing so many thoughts and feelings with me.

It is a pleasure to thank Haye Hinrichsen and Klaus Krebs for their fruitfull and friendly collaboration.

To Michael Proebsting, who shared the office and accepted me the way I am, my warmest thanks.

I am indebt to Dr. Walter Pfeil for his constant support.

I would also like to acknowledge the great help I received from Mrs. Dagmar Faßbender and Mrs. Michaela Mühl.

Last but not least, I thank the DAAD, the Physikalisches Institut der Universität Bonn, and the Federal Ministry for Science and Research for the financial support.

Bibliography

[1] L.P. Kadanoff and J. Swift *Phys. Rev.* **165** (1968) 165

[2] F.C. Alcaraz, M. Droz, M. Henkel and V. Rittenberg, *Ann. Phys.* **230** (1994) 250

[3] V. Privman *Phys. Rev.* **E 50** (1994) 50

[4] K. Kang and S. Redner, *Phys. Rev.* **A 30** (1984) 2833

[5] J. Spouge *Phys. Rev. Lett.* **60** (1988) 871

[6] R. Kroon, H. Fleurent and R. Sprik, *Phys. Rev.* **E 47** (1993) 2462

[7] A.A. Lushnikov *Sov. Phys. JEPT* **64** (1986) 811

[8] C. R. Doering and D. ben-Avraham, *Phys. Rev.* **A 38** (1988) 3035

[9] M. A. Burschka, C. R. Doering and D. ben-Avraham, *Phys. Rev. Lett.* **63** (1989) 700

[10] D. ben-Avraham, M. A. Burschka and C. R. Doering, *J. Stat. Phys.* **60** (1990) 695

[11] C.R. Doering, M.A. Burschka and W. Horsthemke 1991 *J. Stat. Phys.* **65**:953.

[12] D. ben-Avraham, *Mod. Phys. Lett.* **B9** (1995) 895

[13] K. Krebs, M. Pfannmüller, B. Wehefritz and H. Hinrichsen, *J. Stat. Phys.* **78** (1995) 1429

[14] R. J. Glauber, *J. Math. Phys.* **4** (1963) 294;
D. Bedeaux, K. E. Schuler and I. Oppenheim, *J. Stat. Phys.* **2** (1970) 1

[15] I. Peschel, V. Rittenberg, and U. Schultze, *Nucl. Phys.* **B 430** (1994) 633

[16] B. Derrida , E. Domany, D. Mukamel *J. Stat. Phys.* **69** (1992) 667

[17] B. Derrida, M.R. Evans, V. Hakim, V. Pasquier *J. Phys* **A 26** (1993) 1493

[18] G. Schütz, E. Domany *J. Stat. Phys.* **72** (1993) 277

[19] S. Sandow *Phys. Rev.* **E50** (1994) 2660

[20] Fabian H.L. Essler , V. Rittenberg *J. Phys* **A 29** (1996) 3375

[21] K. Krebs, H. Simon, to be published

[22] T. Vicsek, P. Meakin and F. Family, *Phys. Rev.* **A 32** (1985) 1122;
Z. Racz, *Phys. Rev.* **A 32** (1985) 1129;
H. Hayakawa, *J. Phys.* **A 20** (1987) L801;
H. Takayasu, I. Hisikawa and H. Taski, *Phys. Rev.* **A 37** (1988) 3110;

[23] C. R. Doering and D. ben-Avraham, *Phys. Rev. Lett.* **62** (1989) 2563

[24] Z. Cheng, S. Redner and F. Leyvraz, *Phys. Rev. Lett.* **62** (1989) 2321

[25] V. Rittenberg, private comunication

[26] H. Hinrichsen, V. Rittenberg and H. Simon *Universality properties of the stationary states in the one-dimensional coagulation-diffusion model with external particle input*, to appear in *J. Stat. Phys.* **85** (1996)

[27] H. Simon, *J. Phys* **A 28** (1995) 6585

[28] G.M. Schütz *J. Stat. Phys.* **79** (1995) 243

[29] P. Arndt, T. Heinzel and V. Rittenberg, to be published

[30] H. Hinrichsen, K. Krebs and I. Peschel, *Z. Phys.* **B 100** (1996) 105

[31] B. Derrida, V. Hakim and V. Pasquier, *Phys. Rev. Lett.* **75** (1995) 751

[32] B. Derrida, *J. Phys.* **A 28** (1995) 1481

[33] *Handbook of Mathematical Functions*, eds. M. Abramowitz and I.A. Stegun, Dover Publications, New York, 1965

[34] I.S. Gradshteyn and I.M. Ryzhik *Table of Integrals, Series, and Products*, fourth edition, Academic Press, New York, 1965

[35] R. Kopelman *J. Stat. Phys.* **42** (1986) 185

[36] R. Kopelman, S.J. Parus and J. Prasad *J. Chem. Phys.* **128** (1988) 209

[37] W.J. Rodriguez, M.F. Herman, G.L. McPherson *Phys. Rev.* **B 39** (1989) 18

[38] D. Zhong and D. ben-Avraham *J. Phys* **A 28** (1995) 33

[39] V. Privman, C.R. Doering and H.L. Frisch *Phys. Rev.* **E 48** (1993) 846

[40] K. Kang and S. Redner *Phys. Rev. Lett.* **52** (1984) 955

[41] M. Bramson, J.L. Lebowitz *J. Stat. Phys.* **62** (1991) 297

[42] D. Toussaint, F. Wilczek *J. Chem. Phys.* **78** (1983) 2642

[43] B.P. Lee *Critical Behaviour in Non-Equilibrium Systems*, *Ph. D. Thesis*, University of California, Santa Barbara (1993)

[44] J.-C. Lin *Phys. Rev.* **A 44** (1991) 6706

[45] K. Krebs, M. Pfannmüller, H. Simon and B. Wehefritz *J. Stat. Phys.* **78** (1995) 1471

[46] D. ben-Avraham *J. Chem. Phys.* **88** (1988) 941

[47] P. Argyrakis *Computers in Physics* **6** (1992) 525

[48] M. Henkel, *unpublished*

[49] B. P. Lee and J. Cardy, *J. Stat. Phys.* **80** (1995) 971

[50] J. Cardy, private communication

Appendix A

Proof of the equation (3.1.33) in the thermodynamic limit

In this Appendix we prove the integral representation for the one-hole probabilities in the thermodynamic limit (3.1.33):

$$\Omega(x,y) \;=\; 1-\frac{q^{x+y}}{2\pi i}\int_{-\infty}^{+\infty} dz\left(\frac{1}{z}-\frac{z}{z^2+p^2}\right)\left(\mu_z^x\mu_{-z}^y-\mu_z^y\mu_{-z}^x\right). \tag{A.1}$$

Instead of deriving this formula from the finite-size solutions (3.1.24)-(3.1.26) by taking $L\to\infty$ it is much simpler to prove that Eq. (A.1) is a solution of the one-hole equations (3.1.1)-(3.1.4). We first notice that $\Omega(x,x)=1$ because of the antisymmetry of the integrand. In order to verify the bulk equation (3.1.1) let us introduce the notation $g(x,y,z)=q^{x+y}(\mu_z^x\mu_{-z}^y-\mu_z^y\mu_{-z}^x)$. Using Eq. (3.1.31) one can show that

$$q\,g(x-1,y,z)+q^{-1}g(x+1,y,z)+q\,g(x,y-1,z)+q^{-1}g(x,y+1,z)=2(q+q^{-1})g(x,y,z) \tag{A.2}$$

This relation implies that Eq. (A.1) satisfies the bulk equation (3.1.1). The last step is to verify the left boundary condition Eq. (3.1.2). Obviously it is equivalent to prove that

$$\begin{aligned} h(y) \;&=\; q\,\Omega(0,y-1)+q^{-1}\Omega(0,y+1)-(q+q^{-1}+p)\,\Omega(0,y) \\ &=\; -p\;+\;\frac{p^2\,q^y}{2\pi}\int\frac{dz}{z}\Big(\frac{\mu_z^y}{z+ip}+\frac{\mu_{-z}^y}{z-ip}\Big) \end{aligned} \tag{A.3}$$

is equal to zero for all $y=1,2,\ldots\infty$. For $y=0$ we get

$$h(0)\;=\;-p\;+\;\frac{p^2}{2}\int_{-\infty}^{+\infty}dz\,\frac{1}{z^2+p^2}\;=\;0 \tag{A.4}$$

For $y=1$ one has to solve the integrals

$$h(1)\;=\;-p\;+\;\frac{q\,p^2}{2\pi}\left(\int_{-\infty}^{+\infty}dz\,\frac{\mu_z+\mu_{-z}}{z^2+p^2}-\int_{-\infty}^{+\infty}\frac{dz}{z}\,\frac{ip(\mu_z-\mu_{-z})}{z^2+p^2}\right) \tag{A.5}$$

by standard integration techniques in the complex plane. It turns out that all contributions cancel except at $z=0$ in the second integral so that $h(1)=0$. Using Eq. (3.1.31) it is now easy to derive the recurrence relation

$$q^{-1}h(y)\;+\;q\,h(y-2)\;=\;(q+q^{-1})\,h(y-1) \tag{A.6}$$

so that $h(y) = 0$ for $y = 2, 3, \ldots \infty$ follows by induction. This completes the proof of Eq. (A.1). Let us finally consider the case of infinite input rate where Eq. (A.1) reduces to

$$\Omega(x,y) \;=\; 1 - \frac{q^{x+y}}{2\pi i}\int_{-\infty}^{+\infty}\frac{dz}{z}\left(\mu_z^x\mu_{-z}^y - \mu_z^y\mu_{-z}^x\right). \tag{A.7}$$

This expression turns out to be a combination of elliptic integrals. This allows us to compute the particle concentration exactly although the expressions become very complicated as x and y increase. For example the particle concentration in the steady state at the first four sites is given by

$$c(1) \;=\; 1 \tag{A.8}$$

$$c(2) \;=\; \frac{2}{3\pi}\Big[(q^2+1)(1+6q^2+q^4)\mathbf{E} - (q^2+1)(q^2-1)^2\mathbf{K}\Big] - q^2 - 2q^4 \tag{A.9}$$

$$\begin{aligned} c(3) \;=\; & \frac{2}{15\pi}\Big[(q^2+1)(4-15q^2-34q^4-15q^6+4q^8)\mathbf{E} \\ & -(q^2+1)(q^2-1)^2(4-15q^2+4q^4)\mathbf{K}\Big] + 3q^4 - 2q^6 \end{aligned} \tag{A.10}$$

$$\begin{aligned} c(4) \;=\; & \frac{4}{105\pi}\Big[(q^2+1)(12-28q^2+45q^4+238q^6+45q^8-28q^{10}+12q^{12})\mathbf{E} \\ & -(q^2+1)(q^2-1)^2(12-28q^2+69q^4-28q^6+12q^8)\mathbf{K}\Big] - 3q^6 - 4q^8 \end{aligned} \tag{A.11}$$

where

$$\mathbf{E} \;=\; \int_0^{\pi/2} d\theta \left(1 - \frac{4}{(q+q^{-1})^2}\sin^2\theta\right)^{1/2} \tag{A.12}$$

$$\mathbf{K} \;=\; \int_0^{\pi/2} d\theta \left(1 - \frac{4}{(q+q^{-1})^2}\sin^2\theta\right)^{-1/2} \tag{A.13}$$

are elliptic integrals of the first kind.

Appendix B

The stationary density profile for biased diffusion to the right in the continuum limit

In this Appendix we give a proof of equation (3.1.73). We concentrate on the thermodynamical limit of models in which the particle motion is subject to a drift pointing away from the source which is situated at the left boundary ($x = 0$) and we are interested in the large x behavior of the density. The starting point is the contour integral (3.1.50). In the thermodynamical limit the Green function of the Dirichlet problem is defined by the $i = j = 0$ term of the multiple sum of (3.1.55). We are left with two contributions to the holes density function

$$\Omega^c(x,y) \;=\; \Omega^c_\infty(x,y) \;+\; \Omega^c_p(x,y)\,. \tag{B.1}$$

The first one comes from the integration along the diagonal boundary half-line [1] $(0 \le x' = y' < \infty)$

$$\Omega^c_\infty(x,y) \;=\; \frac{|\hat r|}{2\pi} \sum_{\alpha,\beta=\pm 1} (\alpha y - \beta x) \int_0^\infty \frac{K_1(|\hat r| r_1)}{r_1} e^{-\hat r[a-(x+y)/2]}\, da \tag{B.2}$$

where $r_1 = \sqrt{\left(a - \frac{\alpha x+\beta y}{2}\right)^2 + \left(\frac{\alpha x-\beta y}{2}\right)^2}$. This is the holes density function in the case of an infinite input rate.

The second contribution comes from the integration along the left boundary half-line $(0 \le y' < \infty\ ,\ x' = 0)$ and is $\hat p$ dependent

$$\Omega^c_p(x,y) \;=\; \frac{|\hat r|}{\sqrt{2}\pi} \sum_{\alpha=\pm 1} \alpha e^{\hat r(x+y)/2} \int_0^\infty \left\{ y \frac{K_1\!\left(\frac{|\hat r| r_2}{\sqrt 2}\right)}{r_2} - x \frac{K_1\!\left(\frac{|\hat r| r_3}{\sqrt 2}\right)}{r_3} \right\} e^{-\sqrt{\hat r^2/4+\hat p}\ a}\, da \tag{B.3}$$

where $r_2 = \sqrt{\left(a-\alpha x\right)^2 + y^2}$ and $r_3 = \sqrt{\left(a-\alpha y\right)^2 + x^2}$.

The density profile is determined by the holes density function in the limit $y \to x$ (see Eq. (3.1.56)). The behavior of the integrands appearing in (B.2) and (B.3) is given by terms of the form

[1] We note that the derivatives of the Bessel functions with respect to their argument are $K_0'(u) = -K_1(u)$ and $K_1'(u) = -\frac{1}{2}\left(K_0(u) + K_2(u)\right)$

$K_1(u)/u$. For $u \to 0$ the modified Bessel functions diverge like $K_\nu(u) \sim u^{-\nu}$ (for $\mathrm{Re}(\nu) > 0$). The only dangerous term is the one containing r_1 which vanishes for $y \to x$ and $a \to x$ when $\alpha = \beta = 1$. The corresponding term in (B.2)

$$\Omega_0^c(x,y) \;=\; \frac{|\hat{r}|(y-x)}{2\pi} \cdot \int_0^\infty \frac{K_1\left(|\hat{r}|\sqrt{\left(a-\frac{x+y}{2}\right)^2+\frac{(x-y)^2}{4}}\right)}{\sqrt{\left(a-\frac{x+y}{2}\right)^2+\frac{(x-y)^2}{4}}} e^{-\hat{r}[a-(x+y)/2]}\, da \tag{B.4}$$

determines the asymptotic behavior of the particle concentration, in the thermodynamical limit. We start with this term. We use the fact that $K_1(\sqrt{u})/\sqrt{u}$ is the Laplace transform of $\exp(-1/(4t))$ (see Eq. (29.3.122) in ref. [33]). The equation (B.4) can be rewritten

$$\Omega_0^c(x,y) \;=\; \hat{r}^2\frac{y-x}{2\pi} \cdot \int_0^\infty \exp\left(-t\hat{r}^2\left(\frac{x-y}{2}\right)^2\right) dt \int_{-\frac{x+y}{2}}^\infty \exp\left(-t\left(\hat{r}a+\frac{1}{2t}\right)^2\right) da \tag{B.5}$$

After integrating over the variable a we get

$$\Omega_0^c(x,y) \;=\; 1 - \hat{r}\frac{y-x}{2\sqrt{\pi}} \cdot \int_0^\infty \exp\left(-t^2\hat{r}^2\left(\frac{x-y}{2}\right)^2\right) \mathrm{erfc}\left(t\hat{r}\frac{x+y}{2}-\frac{1}{2t}\right) dt \tag{B.6}$$

Here erfc stands for the complementary error function. From (3.1.56) we get that the contribution of $\Omega_0^c(x,y)$ to the particle density is

$$\rho_0(x) \;=\; \frac{\hat{r}}{2\sqrt{\pi}} \cdot \int_0^\infty \mathrm{erfc}\left(t\hat{r}x-\frac{1}{2t}\right) dt \tag{B.7}$$

With the change of variable

$$t \;=\; \frac{\omega+\sqrt{\omega^2+2\hat{r}x}}{2\hat{r}x} \tag{B.8}$$

we get

$$\rho_0(x) \;=\; \frac{1}{2\sqrt{\pi}x}\left(\int_0^\infty \left(1-\frac{\omega}{\sqrt{\omega^2+2\hat{r}x}}\right) d\omega \;+\; \int_0^\infty \frac{\omega}{\sqrt{\omega^2+2\hat{r}x}}\mathrm{erfc}(\omega)\, d\omega\right) \tag{B.9}$$

After integrating by parts one gets

$$\rho_0(x) \;=\; \frac{1}{\pi x}\int_0^\infty \sqrt{\omega^2+2\hat{r}x}\, e^{-\omega^2}\, d\omega \tag{B.10}$$

Expanding in powers of ω^2/x we finally obtain:

$$\rho_0(x) \;=\; \sqrt{\frac{\hat{r}}{2\pi x}} + \frac{1}{8\sqrt{2\pi\hat{r}}}\frac{1}{x^{3/2}} \;+\; O(x^{-5/2}) \tag{B.11}$$

The rest of the holes density function

$$\Omega_{rest}^c(x,y) \;=\; \Omega^c(x,y) - \Omega_0^c(x,y) \tag{B.12}$$

gives also a contribution to the particle density

$$\rho_{rest}(x) \;=\; -\frac{\partial}{\partial y}\Omega^c_{rest}(x,y)\Big|_{y=x} \tag{B.13}$$

In all the integrals contributing to Ω^c_{rest}, the arguments of the Bessel functions (r_i, $i=1,2,3$) are greater then x (or y). We can thus use the asymptotic expansions of $K_\nu(u)$ and replace these functions with $\exp(-u)\cdot\sqrt{\pi/(2u)}$. One obtains an integral expression of $\rho_{rest}(x)$. Due to the exponential falloff of the integrands appearing in (B.13), one can expand them in powers of a/x (where a is the integration variable). After some computations one gets that for $x \to \infty$ $\rho_{rest}(x)$ decays like $x^{-3/2}$.
Summing up we get the following formula for the asymptotic behavior of the density profile

$$\rho(x) \;=\; \sqrt{\frac{\hat{r}}{2\pi x}} + \frac{1}{4\sqrt{2\pi\hat{r}}}\left[\frac{11}{2} - \frac{\hat{r}^4}{\hat{p}^2}\right]\frac{1}{x^{3/2}} \;+\; O(x^{-5/2}) \tag{B.14}$$

We notice that the leading term is independent of the input rate $\hat{p}$ but the next to leading term is $\hat{p}$ dependent.

Appendix C

Details on the Monte Carlo simulations

In this Appendix we explain how we have done the simulations of the coagulation-diffusion model with particle input at one boundary ($p_r = 0$). We can simplify the notation and use the symbol p instead of p_r for the input rate.

The simplest way to simulate reaction-diffusion models is to use a Monte Carlo algorithm with random sequential updates. However, this algorithm is not very efficient for the present problem since particle densities are very low and therefore most of the updates take place at empty sites. This is why we used a different method in which the positions of the particles are stored rather than the occupation numbers of the sites (for details see [45] and references therein). This 'direct' method is much faster than the first one. It is defined as follows. At the beginning the lattice is empty. As long as the total number of particles in the system is 0 the following steps are repeated:

- choose a randomly a number a, between 0 and 1
- occupy site 1 with a particle if $a \leq p\triangle t$
- leave the site unoccupied if $a > p\triangle t$
- increment the time $t \to t + \triangle t$

The parameter $\triangle t$ is the time discretization (see Ref. [45]). After the first particle entered the system, the 'direct' Monte-Carlo algorithm is started:

- choose a *particle* at random and one of its neighboring sites
- update the configuration of the chosen pair with help of a random number and by considering the bulk reaction rates
- increment the time $t \to t + \frac{\triangle t}{N}$ where N is the current total number of particles in the system
- if site 1 is empty try to occupy it by comparing a random number with $p\frac{\triangle t}{N}$. If $p = \infty$ one keeps the site 1 occupied at all time-steps.

In order to test the accuracy of the "direct" Monte Carlo method, we simulated some systems for which analytical data is available. The agreement is very good. For $q = 1$ we used a lattice of length $L = 200$ and took $p = 1$ and $p = 0.01$. Only for the first $10 - 15$ sites the two sets of values for the density profile are slightly different (the relative difference is of less than 10%). For the other sites the difference between the two measurements of the density profile is zero within numerical errors. We also compared data obtained for systems characterized by $q = \sqrt{2.5}$, $L = 20$ sites and $p = 1$ and $p = 0.1$. Although the lattice length is small, the two sets of measurements of the density profiles coincide for all sites within numerical errors.

The quality of the Monte Carlo simulations is higher in the case where the particle diffusion is biased to the right in comparison with the $\Gamma_{01}^{10} \leq \Gamma_{10}^{01}$ case. This has two reasons. On the one hand in the $\Gamma_{01}^{10} > \Gamma_{10}^{01}$ case the total concentration of particles in the stationary state is larger as compared to the symmetric case. It is more likely to reproduce through simulations a distribution with a higher total number of particles. On the other hand the relaxation of these system to the stationary state occurs much faster than in the $\Gamma_{01}^{10} = \Gamma_{10}^{01}$ case since the time operator has massive excitations for $\Gamma_{01}^{10} \neq \Gamma_{10}^{01}$. Therefore less CPU time per run is necessary and thus the numerical errors of the measurements are smaller.

It is a well known fact that the quality of the Monte Carlo determinations is limited by the accuracy of the random number generator. If the number of steps requiring random numbers is too high, at some point the generator produces correlated numbers. This limitation poses some problems in the case of symmetric diffusion, for large lattices. This explains the unphysical oscillations of the data corresponding to $L = 1000$ in Figures 3.3 and 3.4. The choice of a better random number generator implies the increase of the CPU time needed to perform the simulations.

Since we are interested in the stationary properties of the system we stopped each simulation run at a value of $t = t_{max}$ such that at least in the time interval $[t_{max}/3\,, t_{max}]$ the average total number of particles is fluctuating around a constant value. We used a double averaging technique. We took 100 equidistant time points between $[0.9 \cdot t_{max}\,, t_{max}]$ and measured our observables in each of them. For each Monte Carlo run of the program we got a preliminary value by averaging over this 100 determinations. Afterwards we averaged these preliminary values over all MC runs. The number of runs performed for each system was between 4 and 50 thousand, depending on the lattice length. Due to CPU time limitations, the number of runs performed decreases with the lattice length.

For the data presented in Figs. 3.3 and 3.4 we used coarse-graining for obvious reasons, this is reflected in the horizontal error bars.